

1 **Mammalian bioturbation amplifies rates of both hillslope sediment erosion and accumulation**  
2 **along Chilean climate gradient**

3 *Paulina Grigusova*<sup>1</sup>, *Annegret Larsen*<sup>2</sup>, *Roland Brandl*<sup>3</sup>, *Camilo del Río*<sup>4,5</sup>, *Nina Farwig*<sup>6</sup>, *Diana Kraus*<sup>6</sup>,  
4 *Leandro Paulino*<sup>7</sup>, *Patricio Plischoff*<sup>4,8,9</sup>, *Jörg Bendix*<sup>1</sup>

5  
6  
7 <sup>1</sup> Laboratory for Climatology and Remote Sensing, Department of Geography, University of Marburg,  
8 35037 Marburg, Germany; paulina.grigusova@staff.uni-marburg.de (P.G.); bendix@geo.uni-  
9 marburg.de (J.B.)

10 <sup>2</sup> Soil Geography and Landscape, Department of Environmental Sciences,  
11 Wageningen University & Research, 6700 AA Wageningen, The Netherlands; annegret.larsen@wur.nl

12 <sup>3</sup> Animal Ecology, Department of Biology, University of Marburg, 35032 Marburg, Germany;  
13 brandlr@biologie.uni-marburg.de

14 <sup>4</sup> Facultad de Historia, Geografía y Ciencia Política, Instituto de Geografía, Pontificia Universidad Católica  
15 de Chile, 782-0436 Santiago, Chile; cdelriol@uc.cl

16 <sup>5</sup> Centro UC Desierto de Atacama, Pontificia Universidad Católica de Chile, 782-0436 Santiago, Chile

17 <sup>6</sup> Conservation Ecology, Department of Biology, University of Marburg, 35047 Marburg, Germany;  
18 diana.kraus@biologie.uni-marburg.de (D.K.); nina.farwig@biologie.uni-marburg.de (N.F.)

19 <sup>7</sup> Facultad de Agronomía, Universidad de Concepción, 3780000 Chillán, Chile; lpaulino@udec.cl

20 <sup>8</sup> Facultad de Ciencias Biológicas, Departamento de Ecología, Pontificia Universidad Católica de Chile,  
21 8331150 Santiago, Chile; plischoff@uc.cl

22 <sup>9</sup> Center of Applied Ecology and Sustainability (CAPES), Pontificia Universidad Católica de Chile,  
23 8331150 Santiago, Chile; [plischoff@uc.cl](mailto:plischoff@uc.cl)

24

25 Corresponding author:

26 Paulina Grigusova

27 paulina.grigusova@staff.uni-marburg.de

28

29

30

31

32

33

34

35

36

37

38

39

40

41

42 **Abstract**

43 Animal burrowing activity affects soil texture, bulk density, soil water content and redistribution of  
44 nutrients. All of these parameters in turn influence sediment redistribution, which shapes the earth  
45 surface. Hence it is important to include bioturbation into hillslope sediment transport models. However,  
46 the inclusion of burrowing animals into hillslope-wide models has thus far been limited, and largely  
47 omitted vertebrate bioturbators, which can be major agents of bioturbation, especially in drier areas.  
48 Here, we included vertebrate bioturbator burrows into a semi-empirical Morgan-Morgan-Finney soil  
49 erosion model to allow a general approach to for assessing the impacts of bioturbation on sediment  
50 redistribution within four sites along the Chilean climate gradient. For this, we predicted the distribution  
51 of burrows by applying machine learning techniques in combination with remotely sensed data into the  
52 hillslope catchment. Then, we adjusted the spatial model parameters at predicted burrow locations  
53 based on field and laboratory measurements. We validated the model using field sediment fences. We  
54 estimated the impact of bioturbator burrows on surface processes. Lastly, we analyse how the impact  
55 of bioturbation on sediment redistribution depends on the burrow structure, climate, topography, and  
56 adjacent vegetation.

57 Including bioturbation greatly increased model performance and demonstrates the overall importance  
58 of vertebrate bioturbators in enhancing both sediment erosion and accumulation along hillslopes, though  
59 this impact is clearly staggered according to climatic conditions. Bioturbation had contrasting effects on  
60 sediment redistribution in arid than in semi-arid and Mediterranean, as well as in humid climate zone.  
61 Burrowing vertebrates increased sediment accumulation by 137.8 %  $\pm$ 16.4 % in the arid zone (3.53 kg  
62  $\text{ha}^{-1} \text{year}^{-1}$  vs. 48.79 kg  $\text{ha}^{-1} \text{year}^{-1}$ ), sediment erosion by 6.5 %  $\pm$ 0.7 % in the semi-arid zone (129.16 kg  
63  $\text{ha}^{-1} \text{year}^{-1}$  vs. 122.05 kg  $\text{ha}^{-1} \text{year}^{-1}$ ) and sediment erosion by 15.6 %  $\pm$ 0.3 % in the Mediterranean zone  
64 (4602.69 kg  $\text{ha}^{-1} \text{year}^{-1}$  vs. 3980.96 kg  $\text{ha}^{-1} \text{year}^{-1}$ ). Bioturbating animals seem to play only a negligible  
65 role in the humid zone. Within all climate zones, bioturbation did not uniformly increase erosion or  
66 accumulation within the whole hillslope catchment. This depended on adjusting environmental  
67 parameters. Bioturbation increased erosion with increasing slope, sink connectivity and topography  
68 ruggedness, decreasing vegetation cover and soil wetness. Bioturbation increased sediment  
69 accumulation with increasing surface roughness, soil wetness and vegetation cover.

70  
71  
72  
73  
74  
75  
76  
77  
78  
79  
80  
81  
82

## 83 1. Introduction

84 Bioturbation was shown to shape the land surface (Hazelhoff et al., 1981; Istanbuluoglu, 2005; Taylor  
85 et al., 2019; Tucker and Hancock, 2010; Whitesides and Butler, 2016; Wilkinson et al., 2009; Corenblit  
86 et al., 2021) by influencing surface microtopography (Reichman and Seabloom, 2002; Kinlaw and  
87 Grasmueck, 2012; Debruyne and Conacher, 1994), and soil properties such as soil porosity, permeability  
88 and infiltration (Reichman and Seabloom, 2002; Yair, 1995; Hancock and Lowry, 2021; Ridd, 1996; Hall  
89 et al., 1999; Coombes, 2016; Larsen et al., 2021). Cumulatively, these modifications lead to changes in  
90 sediment redistribution (Gabet et al., 2003; Nkem et al., 2000; Wilkinson et al., 2009) and hence have  
91 the potential to affect surface topography and nutrient redistribution on large spatial and temporal scales.  
92 To quantify these effects, the shared role of climate, landscape characteristics and burrowing dynamics  
93 on sediment redistribution needs to be understood.

94 On a local scale, currently used field methods to monitor sediment redistribution under real-life condition  
95 are mainly erosion pins, splash boards, or rainfall simulators (Imeson and Kwaad, 1976; Wei et al., 2007;  
96 Le Hir et al., 2007; Li et al., 2019a; Li et al., 2019b; Li et al., 2018; Voiculescu et al., 2019; Chen et al.,  
97 2021; Übernickel et al., 2021a). The monitoring of box experiments yields a high spatio-temporal  
98 resolution, and can also be linked with mathematical equations, such as random walks (Boudreau, 1986;  
99 Wheatcroft et al., 1990), stochastic differential equations (Boudreau, 1989; Milstead et al., 2007), finite  
100 difference mass balancing (Soetaert et al., 1996; François et al., 1997) or Markov chain theory (Jumars  
101 et al., 1981; Foster, 1985; Trauth, 1998; Shull, 2001) to describe sediment redistribution.

102 Previously used methods have, however, several limitations when studying bioturbation. Field  
103 measurements likely lead to an underestimation of sediment fluxes, as they are one-time or seasonal  
104 measurements, and thus do not capture the continuous excavation of the sediment by the animal  
105 (Grigusova et al., 2022) at a high temporal resolution. Box experiments and from them derived  
106 mathematical equations describe bioturbation as an isolated process and ignore adjacent environmental  
107 parameters (such as climate or vegetation). However, the field measurements showed both, positive  
108 (Hazelhoff et al., 1981; Black and Montgomery, 1991; Chen et al., 2021) and negative impact of  
109 bioturbation on erosion (Imeson and Kwaad, 1976; Hakonson, 1999). Also, previous field based studies  
110 observed an increased bioturbation activity with higher (Milstead et al., 2007; Meserve, 1981; Tews et  
111 al., 2004; Wu et al., 2021; Ferro and Barquez, 2009), but also with lower vegetation cover (Simonetti,  
112 1989; Zhang et al., 2020; Zhang et al., 2019; Qin et al., 2021). Furthermore, soil mixing rates are not  
113 homogenous throughout the year but depend on the animal phenological cycles (Eccard and Herde,  
114 2013; Jimenez et al., 1992; Katzman et al., 2018; Malizia, 1998; Morgan and Duzant, 2008; Monteverde  
115 and Piudo, 2011; Gray et al., 2020; Yu et al., 2017).

116 Another approach offer raster-based soil erosion and landscape evolution models which integrate co-  
117 dependencies between bioturbation relevant environmental parameters (Black and Montgomery, 1991;  
118 Meysman et al., 2003; Yoo et al., 2005; Schiffers et al., 2011). Most common soil erosion models are  
119 empirical (Wischmeier and Smith, 1978; Williams, 1975; Renard et al., 1991), process-based (Morgan  
120 et al., 1998; ROO et al., 1996; Nearing et al., 1989; Beasley et al., 1980), or semi-empirical models, the  
121 latter of which are a combination of both (Morgan et al., 1984; Beven and Kirkby, 1979).

122 **Process-based models are based on a mechanistic understanding of the underlying physical, chemical,**  
123 **and biological processes that govern the behaviour of the system being studied. They must be**

124 parametrised for each site; however, these models explicitly represent the governing equations and  
125 simulate the system's behaviour by numerically solving these equations. Process-based models are  
126 generally considered to be more realistic and accurate than empirical models because they capture the  
127 fundamental processes that drive the system's behaviour. However, process-based models can be  
128 computationally expensive, require more data and knowledge of system properties, and may require  
129 complex numerical algorithms (Morgan et al., 1998; ROO et al., 1996; Nearing et al., 1989; Beasley et  
130 al., 1980).

131 Within empirical models, on the other hand, the physical equations are completely replaced by  
132 empirically determined equations which only hold for the specific area they are derived for. These  
133 models are generally simpler, less computationally expensive, and require more data and knowledge of  
134 system properties than process-based models. However, empirical models also tend to be less accurate  
135 than process-based models, particularly when applying beyond the range of data used to fit the model.  
136 In contrast to physical-based models, empirical models may not be applicable to new or different  
137 conditions, as they are based on observed relationships and do not capture the underlying processes  
138 that govern system behaviour (Wischmeier and Smith, 1978; Williams, 1975; Renard et al., 1991).

139 Semi-empirical models combine the advantages of the both model types (Morgan et al., 1984; Morgan,  
140 2001; Morgan and Duzant, 2008; Devia et al., 2015; Lihare et al., 2015).

141 Most landscape models do not yet implement impacts of bioturbators on water and sediment fluxes  
142 (Brosens et al., 2020; Anderson et al., 2019; Braun et al., 2016; Cohen et al., 2015; Cohen et al., 2010;  
143 Carretier et al., 2014; Welivitiya et al., 2019). There are numerous models describing benthic soil mixing  
144 (Francois et al. 1997, Francois et al. 2002, Kadko and Heath 1984, Croix et al. 2002), biodiffusion caused  
145 by all invertebrate bioturbators (Maysman et al. 2005, Rakotomalala et al. 2015, Morris et al. 2006) or  
146 vertical soil mixing and lateral sediment redistribution caused by single invertebrate species (Orvain et  
147 al. 2006, Román – Sánchez et al. 2019, Orvain 2005, Orvain 2003, Sanford 2008). However, there are  
148 also models which described the impact of bioturbation on sediment redistribution by the vertebrate  
149 animal species: such as the impact of pocket gophers on non-linear hillslope diffusion (Gabet 2000) or  
150 on the creation of Mima mounds (Gabet et al. 2014). Several models include soil vertical mixing caused  
151 by bioturbation and its effect on landscape evolution on a millennial scale. This rather large spatio-  
152 temporal scale however means an omission of the natural variability in burrow sizes and densities,  
153 climate zones and seasonality. In these models, soil erosion is proportionally increasing with increasing  
154 bioturbation, vertical soil mixing rates are uniform, and bioturbation is positively linked with vegetation  
155 cover (Temme and Vanwalleghem, 2016; Vanwalleghem et al., 2013; Yoo and Mudd, 2008; Pelletier et  
156 al., 2013). None of the previous studies included vertebrate bioturbator burrows of various sizes and  
157 spatial distribution by adjusting the soil properties and topography into a raster-based area-wide soil  
158 erosion model. This approach would enable to understand impact of all vertebrate bioturbators by  
159 considering the spatial distribution and variable impacts of bioturbator burrows on sediment  
160 redistribution. For this, bioturbation has to be included into erosion models at a spatial resolution which  
161 allows to imitate the surface processes occurring within and near the burrow, and at a temporal  
162 resolution which captures the animal daily burrowing behaviour.

163 A suitable model which can be extended to include continuous bioturbating activity is the semi-empirical  
164 Morgan – Morgan – Finney soil erosion model (Morgan et al., 1984; Morgan, 2001). This model was

165 successfully tested in several climate zones and land use types, such as Mediterranean sites (Jong et  
166 al., 1999), rainfed agrosystems, fields and pastures (López-Vicente et al., 2008), East-African Highlands  
167 (Vigiak et al., 2005) or humid forests (Vieira et al., 2014). One of the recently developed improvements  
168 of this model is the Daily Morgan – Morgan – Finney model (DMMF), which introduces subsurface flow,  
169 vegetation structures (type, size, height, root depth), and enables modelling at a high spatial (0.5 m) and  
170 temporal (daily) resolution (Choi et al., 2017). These improvements yield the potential to integrate the  
171 bioturbation into the model, as the burrowing activity is not constant and depends on vegetation structure  
172 (Tews et al., 2004; Ferro and Barquez, 2009).

173 In this study, we include vertebrate bioturbator burrows into a semi-empirical soil erosion model (DMMF)  
174 at a daily temporal and 0.5 m spatial resolution. For this, we predict the distribution of burrows by  
175 applying machine learning techniques in combination with using remotely sensed data as predictors.  
176 Then, we adjust soil properties, topography and vegetation properties at predicted burrow locations  
177 based on field and laboratory measurements. We validate the model using field sediment fences. We  
178 run the model for a time period of 6 years, once with and without burrow adjustments. We estimate the  
179 impact of bioturbator burrows on sediment redistribution (including accumulation, erosion, and  
180 excavation), and surface runoff within four sites along the Chilean climate gradient. Lastly, we analyse  
181 how the impact of bioturbation on sediment redistribution depends on the burrow structure, climate,  
182 topography, and adjacent vegetation. Our study shows the importance of including bioturbation into  
183 erosion modelling, and describes the interplay between bioturbation, environmental parameters such  
184 as... and sediment redistribution.

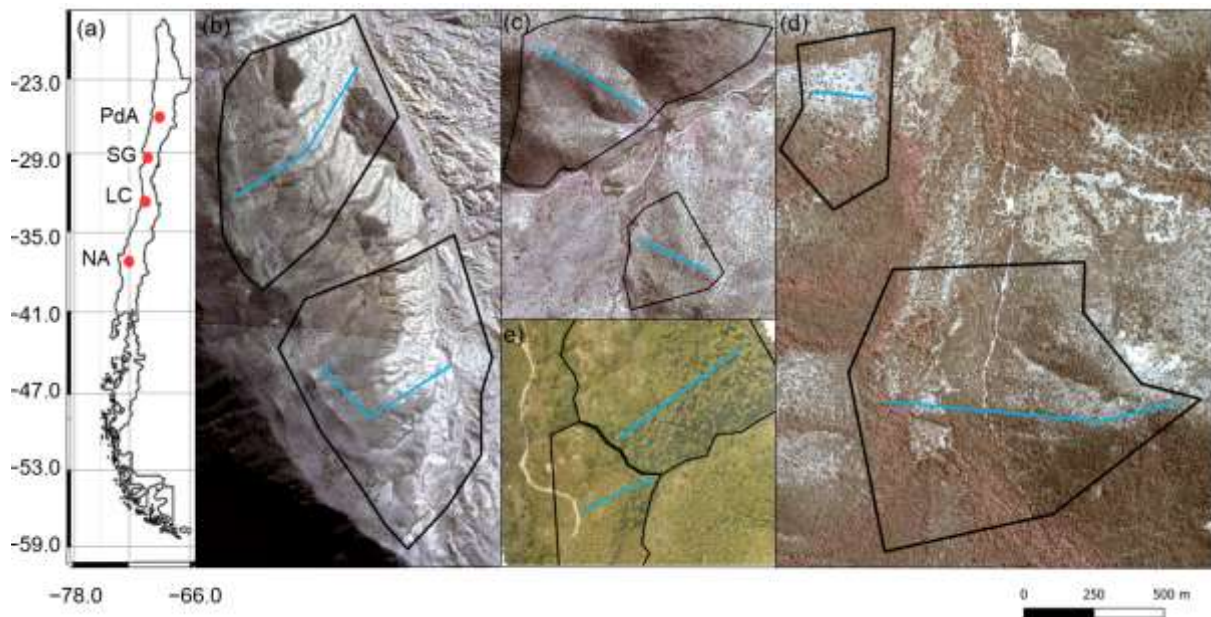
185

## 186 2. Study area

187 Our study was performed along a climate and vegetation gradient in Chile (Übernicket et al., 2021b),  
188 comprising four study sites in the Chilean Coastal Cordillera: Pan de Azúcar (PdA) National Park (NP),  
189 Santa Gracia (SG), La Campana (LC) NP, and Nahuelbuta (NA) NP (Fig. 1). PdA NP is located in the  
190 arid zone in a fog-laden environment in the southern part of the Atacama Desert, with almost no rainfall.  
191 The vegetation cover is less than 5 % and dominated by small desert shrubs, several types of cacti and  
192 biocrusts (Lehnert et al., 2018). SG is a natural reserve located in the semi-arid zone near La Serena,  
193 which is dominated by goat grazing. The vegetation consists of shrubs and cacti, covering up to 40 %  
194 of the study area. LC NP is part of the Mediterranean-type climate zone in the Valparaiso Region and is  
195 also affected by cattle. The study site is dominated by an evergreen sclerophyllous forest with endemic  
196 palms. The canopy reaches a height of up to 9 m, and the understory consists of deciduous shrubs and  
197 herbs. NA is located in the humid-temperate zone and characterized by a dense evergreen *Araucaria*  
198 forest comprising broadleaved trees with heights of up to 14 m. The ground is covered by bamboo,  
199 shrubs, and herbs (Bernhard et al., 2018; Oeser et al., 2018). The most common bioturbating vertebrate  
200 animal species recorded within these sites are carnivores of the family Canidae (*Lycalopex culpaeus*,  
201 *Lycalopex griseus*) as well as rodents of the families Abrocomidae (*Abrocoma bennetti*), Chnichillidae  
202 (*Lagidium viscacia*), Cricetidae (*Abrothrix andinus*, *Phyllotis xanthopygus*, *Phyllotis limatus*, *Phyllotis*  
203 *darwini*) and Octogontidae (Cerqueira, 1985; Jimenez et al., 1992; Übernicket et al., 2021a).

204



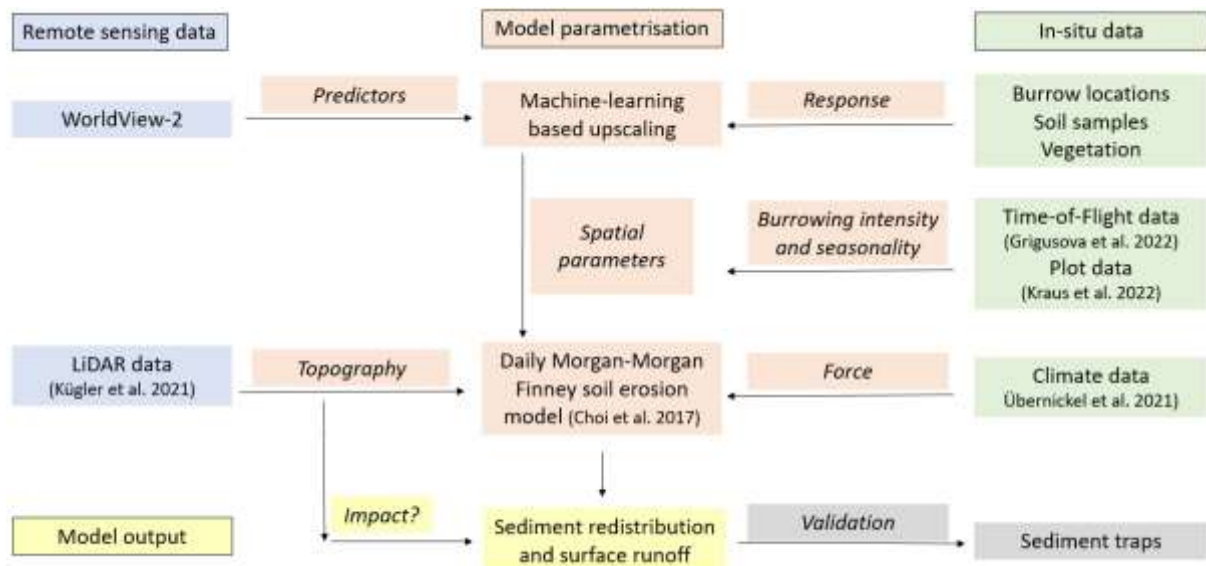


205  
 206 **Figure 1.** Study area and study sites. Black lines outline the hillslope catchments. Along the blue lines,  
 207 the in situ data (mound locations, soil samples, vegetation mapping) were collected. (a) Position of the  
 208 study sites along the climate gradient. PdA = Pan de Azúcar, SG = Santa Gracia, LC = La Campana,  
 209 NA = Nahuelbuta; Positions of plots in (b) PdA; (c) SG; (d) LC; and (e) NA. The background image is an  
 210 RGB-composite calculated from WorldView-2 satellite imagery. Images were obtained with single  
 211 license from GAF AG. Scale bar is the same for (b), (c), (d) and (e).

212  
 213 **3. Methodology**

214 We combined semi-empirical soil erosion modelling with in-situ measurements, remote sensing data  
 215 and machine learning methods (Fig. 2). Along 8 hillslope catchments within 4 climate zones we mapped  
 216 locations of burrows, estimated the vegetation cover and extracted soil samples. We analyzed the soil  
 217 samples in the laboratory. Then we used remote sensing datasets and machine learning to upscale  
 218 burrow distribution, vegetation cover and soil properties into the hillslope catchments. The hillslope  
 219 catchment-wide predictions, the topographical information retrieved from LiDAR data (Kügler et al.,  
 220 2022) and the climate information retrieved from climate stations were the input parameters for our soil  
 221 erosion model. We ran the model with and without bioturbation. We included the bioturbation into the  
 222 model by adjusting the input parameters at the predicted burrow locations, by including the continuous  
 223 burrowing activity and soil mixing (Grigusova et al., 2021), and the seasonality (Kraus et al., 2022).and  
 224 the animal phenological cycle as found in (Jimenez et al., 1992). The models were validated using self-  
 225 constructed sediment traps. We studied the modeled surface runoff and sediment redistribution. Lastly,  
 226 we analyzed if and how the impact of bioturbation on sediment redistribution depends on environmental  
 227 parameters (topography, landscape connectivity and vegetation).

228  
 229



230

231 **Figure 2.** Flow chart of our study. Green color indicates in-situ input data, blue indicates remote sensing  
 232 input data. Red indicates Model parametrization. Yellow indicates model output and analysis. Grey  
 233 indicates model validation.

234

### 235 3.1 In-situ data

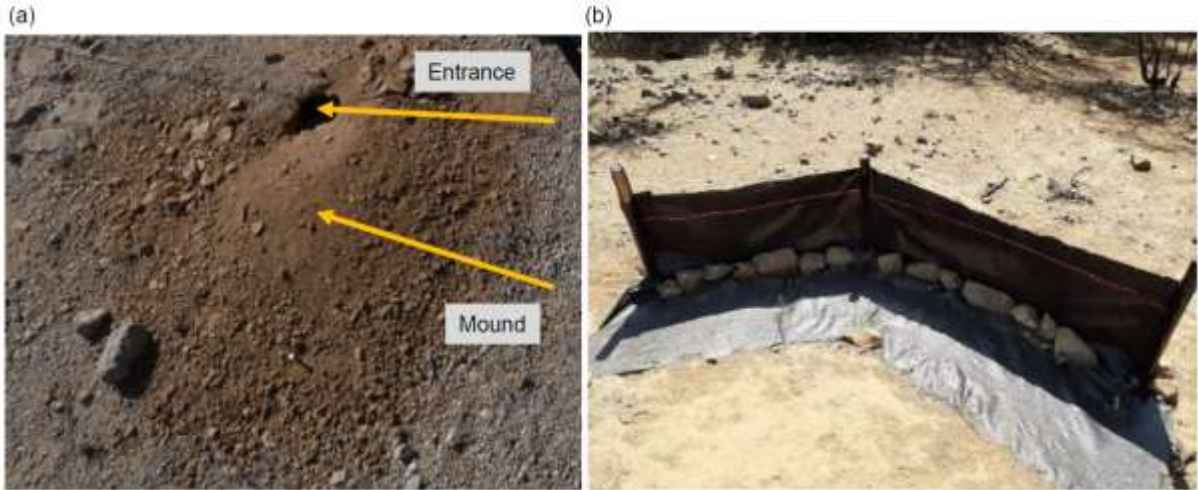
236 The study set-up consisted of eight hillslope catchments: one north-facing and one south-facing hillslope  
 237 catchment per study site. We defined a line with a width of one meter from the top to the base of each  
 238 hillslope catchment (see blue line, Fig. 1). We subdivided the track into tiles of 1 m<sup>2</sup>. We saved the GPS  
 239 information of each tile.

240 Within each tile of the line, we mapped burrow presence, land cover and extracted soil samples. A  
 241 burrow consisted of an entrance and a mound (Fig. 3a). Each 1 m<sup>2</sup> tile with a burrow was described as  
 242 a presence data point, tiles without a burrow as absence data points. We noted the size of the burrow,  
 243 vegetation cover and land cover types (bare soil, herbs, shrubs, trees) within the tile. We extracted 162  
 244 soil samples from soil without a mound at a depth of 10 cm. Additionally, we took a photo of the surface  
 245 every second tile along the track.

246 To validate the model output, we set up sediment traps (Fig. 3b), with six traps per site, two of which  
 247 were located at the hillslope catchment base and four were located on two random positions within the  
 248 hillslope catchment. The sediment traps consisted of geotextile vertically attached to wooden poles for  
 249 stability. The traps had a length of 2 m – 5 m, a width of ~1.5 m and a height of ~1 m. 1.5 m of geotextile  
 250 was laid down at the surface uphill the wooden poles to enable the collection of sediment. The sediment  
 251 accumulated within the traps was collected after 1 year and its mass [cm<sup>3</sup>] and dry weight [kg] were  
 252 estimated.

253 Climate information was retrieved from climate stations located adjacent to the hillslope catchments  
 254 which provide climate data in 5 minute intervals (Übernicket et al. 2021). To force the model on an hourly  
 255 basis, hourly air temperature, precipitation total and intensity, wind speed, wind direction and humidity  
 256 was calculated for the study period from 1<sup>st</sup> April 2016 to 1<sup>st</sup> December 2021. Evapotranspiration was  
 257 estimated by the Penman-Monteith equation (Penman, 1948).

258



259  
 260 **Figure 3.** In-situ constructions. (a) Example of a burrow consisting of burrow entrance and mound. (b)  
 261 Fence construction used for the collection of eroded sediment to validate the model. Both photos by  
 262 Paulina Grigusova.

263

### 264 3.2 Estimation of soil properties

265 We estimated several soil properties from the soil samples and photos collected in-situ ( Grigusova et  
 266 al., 2022). We estimated the rock coverage on the surface and debris from the photos taken every  
 267 second tile. For this, the photos were firstly classified into 5 classes. The classification was unsupervised  
 268 using k-means (Fig. A1). Then we calculated the ratio of pixels classified as skeleton and / or debris to  
 269 the overall amount of all pixels to determine the amount of both parameters in percent.

270 In the lab, we estimated soil water content, bulk density, soil particle density, soil texture (sand, silt, clay,  
 271 coarse / middle / fine sand, coarse / middle / fine silt), soil skeleton, organic matter and organic carbon.  
 272 Gravimetric soil water content [%] (GSWC) described the mass of water within the soil sample and was  
 273 estimated as in Eq (1):

$$274 \text{GSWC} = \frac{(S_m - S_d)}{S_d} * 100 \quad , \quad (1)$$

275 where  $S_m$  [g] is the mass of moist soil measured directly after the extraction and  $S_d$  [g] is the mass of  
 276 soil dried at 105 °C for at least 24 hours. Bulk density [g cm<sup>-3</sup>] (BD) was calculated as following:

$$277 \text{BD} = \frac{S_d}{S_v} \quad , \quad (2)$$

278 where  $S_v$  [cm<sup>-3</sup>] is the volume of the sample. Soil particle density [g cm<sup>-3</sup>] (SPD) was calculated as in Eq  
 279 (3):

$$280 \text{SPD} = \frac{d_m}{S_v} \quad , \quad (3)$$

281 where  $d_m$  [g] is the dry mass of soil particles excluding pores.

282 Particle size distribution [%] – clay (< 0.002 mm), coarse, middle and fine silt (0.002 mm to 0.02 mm),  
 283 and coarse, middle and fine sand (0.02 mm to 2 mm) was estimated using a PARIO method (Durner et  
 284 al., 2017). Soil skeleton was estimated as the ratio of particles with a diameter above 2 mm. Ratio of  
 285 organic matter (OM) was estimated as in Eq. (4)

$$286 \text{OM} = 1 - \frac{S_c}{S_d} \quad , \quad (4)$$

287 where  $S_c$  is the weight [g] of the sample dried at 500 °C for 16 hours.



288 We used pedotransfer functions to determine porosity, saturated soil moisture, hydraulic conductivity,  
 289 water content at field capacity, and permanent wilting point. Pore ratio ( $\theta_s$ ) was estimated from bulk and  
 290 particle density as in Eq. (5):

$$291 \theta_s = \frac{BD}{SPD} \quad (5)$$

292 Saturated water content [ $\text{g g}^{-1}$ ] ( $W_s$ ) was estimated as in Eq. (6):

$$293 W_s = \theta_s \frac{p_w}{BD} \quad (6)$$

294 where  $p_w$  [ $\text{g cm}^{-3}$ ] is the density of water which is set to be  $1 \text{ g cm}^{-3}$  (Pollacco, 2008).

295 Hydraulic conductivity  $K_s$  [ $\text{m s}^{-1}$ ] was estimated as in Eq. (8):

$$296 K_s = 1.15741 * 0.0000001 * \exp(x) \quad (7)$$

297 where  $x$  for sandy soil is:

$$298 x = 9.5 - 1.471 * (BD * BD) - 0.688 * OM + 0.0369 * (OM * OM) - 0.332 * CS \quad (8)$$

299 and  $x$  for loamy and clayey soils is:

$$300 x = -43.1 + 64.8 * BD - 22.21 * (BD * BD) + 7.02 * OM - 0.1562 * (OM * OM) + 0.985 * \ln(OM) -$$

$$301 0.01332 * C * OM - 4.71 * BD * CS \quad (9)$$

302 where  $C$  is percentage of clay and  $CS$  is percentage of clay and silt (Wösten, 1997). To estimate water  
 303 content at field capacity [%] (FC) and permanent wilting point (PWP), we applied functions by (Tomasella  
 304 et al., 2000) as these were developed for South American soils:

$$305 FC = 4.046 + 0.426 * Si + 0.404 * C \quad (10)$$

$$306 PWP = 0.91 + 0.15 * Si + 0.396 * C \quad (11)$$

307 where  $Si$  is the percentage of silt.

308

### 309 3.3 Processing of remote sensing data

310 The digital elevation models (DEM) were calculated from the LiDAR data (Kügler et al., 2022; Horn,  
 311 1981) at a resolution of 0.5 m. Slope was calculated according to Horn (1981). Manning's surface  
 312 roughness coefficient was estimated following (Li and Zhang, 2001). Topographic position index (TPI)  
 313 and Topographic ruggedness index (TRI) were calculated according to (Wilson et al., 2007). **TPI subtract**  
 314 **the mean elevation of pixels in a specified range from the elevation of the central pixel. Positive values**  
 315 **represent hills while negative values represent valleys. The TRI adds together the elevation differences**  
 316 **between a grid cell and its eight neighbours. It measures the relative level of topography irregularity, the**  
 317 **higher the value, the more irregular the topography.** Plan and profile curvature were determined after  
 318 (Zevenbergen and Thorne, 1987). Connectivity indices, Sinks, Wetness index, Flow direction, Flow path,  
 319 Catchment slope and Catchment were calculated in SAGA GIS.

320 Single license stereo WorldView-2 images with a resolution of 0.5 m were retrieved from GAF Munich  
 321 GmbH. The topographic correction of WorldView-2 images was done using the LiDAR data, solar  
 322 elevation angle, solar zenith angle and azimuth angle according to Goslee (2019). The digital surface  
 323 models (DSMs) were calculated from the stereo images. Additionally, we extracted single bands and  
 324 calculated the normalized difference vegetation index (NDVI).

325

### 326 3.4 The erosion model

#### 327 3.4.1 Daily Morgan-Morgan-Finney model

328 The DMMF model is a combined soil erosion model used to estimate surface runoff and sediment flux  
329 on a field scale on a daily basis. Spatially, the DMMF model represents an area as several  
330 interconnected elements (e.g. pixels) of uniform topography, soil characteristics, land cover type, and  
331 vegetation structure. Through coupling, the model operates with flow direction algorithms: each element  
332 receives water and sediments from upslope elements and delivers the generated surface runoff and  
333 eroded soils to downslope elements. On a temporal scale, the model estimates surface runoff and  
334 sediment flux of each element on a daily basis. The model input parameters include climate, topography,  
335 soil properties and land cover information (Choi et al., 2017). Data pre-processing, modelling and  
336 analysis (see Fig. 2) was done in R statistic environment. The raster data were cropped to the size of  
337 the hillslope catchments (Fig. 1). Input parameters are listed in Table 1 and plotted in Fig. A2.

338 During the model simulation, water and sediment are transferred from pixels located at higher elevations  
339 to pixels situated at lower elevations. This occurs in two stages: The first stage is the hydrological phase  
340 where the model calculates surface runoff which happens when the amount of surface water input  
341 exceeds the water-holding capacity. The amount of surface runoff is computed by taking the infiltration  
342 capacity of the surface, the volume of surface water input, and the fraction of the impervious area of a  
343 pixel into account. Infiltration capacity represents the maximum amount of surface water that can  
344 penetrate the subsurface layer. It is determined by the percentage of the impervious area and the  
345 available pore space.

346 The second stage is the sediment phase, where the model estimates the sediment budget for each  
347 particle size class, based on the surface conditions. The model calculates the detachment and  
348 deposition of sediments in a step-by-step process. The sources of sediments are detached particles  
349 from the pixel itself due to rainfall and surface runoff, and delivered soil particles from higher elevation  
350 pixels. The detachment of soil particles by rainfall occurs when raindrops hit the ground with enough  
351 energy to detach soil particles from the surface. Rainfall has different impacts on areas with and without  
352 canopy cover, as canopy cover changes the kinetic energy of raindrops.

353 The amount of soil particles detached by raindrops is calculated based on the soil particle detachability,  
354 the percentage of each particle size class, the bare soil surface area, and the kinetic energy of effective  
355 rainfall. The amount of detached soil particles by surface runoff is calculated based on the soil particle  
356 detachability, the amount of runoff, the slope angle of the pixel, and the proportion of the bare surface  
357 area. The third source of sediment is from higher elevation pixels and is averaged by the surface area  
358 of the pixel.

359 Once sediments are delivered to the surface runoff, a portion of the suspended sediments settles to the  
360 bottom due to gravitational force. To calculate this settling, the model requires the flow velocity of the  
361 runoff and the settling velocity of each particle size class, which are influenced by the flow depth, slope  
362 angle of the pixel, and Manning's roughness coefficient (Choi et al. 2019).

363

#### 364 **3.4.2 Estimation of spatial parameters**

365 For spatial parameterization of the DMMF model, we predicted land cover, soil properties and burrow  
366 distribution onto the hillslope catchments using machine learning techniques.

367 We used the approach Meyer et al. 2018. The most important predictors were selected by forward  
368 feature selection. The quality of the random forest models was assessed by Leave-Location-Out cross

369 validation. We trained the model stepwise, using in-situ data collected from seven of the hillslope  
370 catchments and validated the model using in-situ data from the remaining hillslope catchment (Meyer et  
371 al., 2018). The prediction was done at 0.5 m spatial resolution. We used the WorldView-2 layers obtained  
372 with a single license from GAF, NDVI, DEM, DSM, slope and roughness as predictors. The PAN-  
373 sharpening of the WV-2 layers was done by GAF.

374 For the area-wide prediction of burrow locations across the hillslope catchments, we used the burrow  
375 presence and absence data (section 3.1) as the response data within the RF models. The accuracy was  
376 0.82 for PdA, 0.77 for SG, 0.75 for LC and 0.85 for NA. The prediction of soil properties was done using  
377 soil properties estimated along the track line (see section 3.1) as response data within the RF models.  
378 All of the models reached a high accuracy (see Table A1).

379 To obtain land cover classification, we used as the response within the RF models the land cover  
380 measured in-situ. The classes were soil without rocks, rocks, biocrusts, grass/herbs, shrubs and trees.  
381 Predictor values for each class were extracted from at least 100 polygons per site and class. The  
382 accuracy of the RF models was 0.71 for PdA, 0.81 for SG, 0.83 for LC and 0.75 for NA.

383 The vegetation height measured in plots was averaged for each class per site. All pixels classified as  
384 respective class were assigned the same vegetation height information. Vegetation density was  
385 estimated per hillslope catchment as the amount of vegetation individuals per m<sup>2</sup>. Vegetation diversity  
386 was calculated by Shannon index (Shannon, 1948). The interception area was the area not covered by  
387 vegetation (herbs, shrubs or trees).

388

389

### 390 **3.4.3 Inclusion of bioturbation**

391 In the grid cells with predicted burrow locations, we adapted the values of input parameters to include  
392 bioturbation. The adaptations varied with climate zone and burrow size. The size, geometric structure  
393 and excavation rates of burrowing animals were previously estimated at a high spatial and temporal  
394 resolution (Grigusova et al., 2022). Based on this results, we firstly adjusted the microtopography. We  
395 modified the layer depth to represent burrow entrance and elevation to represent animal mound. Mounds  
396 were always located downslope of burrow entrances in the direction of flow.

397 Secondly, we adjusted the soil properties. Soil properties texture and organic carbon were estimated  
398 from soil extracted from mounds in Kraus et al. (2022). In this study we additionally estimated bulk  
399 density, initial water content, soil skeleton, porosity, saturated water content, available water capacity  
400 and water content at field capacity from the same dataset (see section 3.2). We calculated the median  
401 value of each property for the samples extracted from mounds and for the samples extracted from soil  
402 without mounds. Then, we estimated the change in percent between these two values. This was then  
403 used to adjust the soil property for each pixel including a mound.

404 Thirdly, modelled mound pixels had to be cleared from ground vegetation cover. For this, we removed  
405 ground vegetation cover from pixels with burrow locations and decreased ground vegetation cover,  
406 height, diameter and amount of ground vegetation individuals from adjacent pixels as measured in situ.  
407 Then, the amount of rocks and debris was set as estimated from soil samples (section 3.2)

408 Animal activity has been found to be highly variable throughout the year (Grigusova et al., 2022; Kraus  
409 et al., 2022). The density of burrows does not stay stable throughout the year but increases or decreases

410 depending on the season and climate zone. We therefore artificially removed or added burrows into the  
 411 hillslope catchments at the particular seasons. For this, we adapted the density of soil, the topography  
 412 and vegetation cover accordingly. We created a 3D-model of the burrow structure, adjusted subsurface  
 413 soil properties and properties of soil excavated to the surface; the removed vegetation within the pixel  
 414 with a predicted burrow and decreased adjacent vegetation cover. Animal burrowing activity varies  
 415 throughout the course of the year, and there is a three-month period during which they are mostly active,  
 416 which we considered using/doing xxx

417 Lastly, we also included the vertical movement of sediment particles from deeper soil layers to the  
 418 surface in dependence on climate. Animals were found to reconstruct their burrows after each rainfall  
 419 event (Grigusova et al., 2022). Corresponding with these findings, we increased the entrance depth and  
 420 mound height by 30% after each rainfall event, which represents the averaged value found in the  
 421 previous study (Grigusova et al., 2022).

422 For the validation, we ran the model for the time periods between the installation of sediment fences  
 423 and the collections of sediment. We compared the mass and weight of modelled and collected sediment  
 424 and estimated R<sup>2</sup> and RMSE. To test the importance of the inclusion of individual bioturbation  
 425 parameters into the model, we ran the model under 4 conditions: (i) No burrows; (ii) Solely entrances;  
 426 (iii) Solely mounds; (iv) Entire burrows (entrances and mounds).

427

428 **Table 1.** Model input layers and respective changes to layer values at the predicted burrow locations.  
 429 Ground vegetation was removed from the respective pixels, while tree canopy was not changed. The  
 430 values were estimated as described in 3.5.2. Using the adjusted values, we calculated  
 431 evapotranspiration using the Penman-Monteith equation, surface roughness from the elevation layer,  
 432 and hydraulic conductivity, water content at field capacity and saturated water content using  
 433 pedotransfer functions.

Derivation	Parameter	Units	Pixel value at burrow locations			
			PdA	SG	LC	NA
DEM	Elevation	m asl	+0.24	+0.23	+0.36	+0.19
	Surface roughness	-	-	-	-	-
	Depth	m	-0.23	-0.41	-0.22	-0.04
Soil samples	Water content	%	+120	-6	-68	-62
	Bulk density	g cm <sup>-3</sup>	-	-6	-17	-
	Sand	%	-29	-12	+57	-43
	Silt	%	+54	+22	+23	ns
	Clay	%	+145	+44	+19	-73
	Organic carbon	%	+168	+72	+105	+25
Pedotransfer functions	Hydraulic conductivity	m s <sup>-1</sup>	-	-	-	-
	Water content at field capacity	%	-	-	-	-
	Saturated water content	%	-	-	-	-
	Ground vegetation cover	%	0	0	0	0

Land cover classification	Soil and debris	%	100	100	100	100
	Skeleton	%	0	0	0	0
	Average plant height	m	0	0	0	0
	Average plant diameter	m	0	0	0	0
	Number of plants	n m <sup>-2</sup>	0	0	0	0

434

### 435 **3.5 DMMF model sensitivity test**

436 We conducted a sensitivity test to identify those input parameters which significantly influence the model  
437 output. For this, we first estimated the mean value of each input parameter. Then, we created an artificial  
438 hillslope catchment of 100 m \* 100 m. To start the test, each pixel received the mean value of each  
439 parameter. We ran the model for one rainfall event. Then, we stepwise changed the single input  
440 parameter values from their minimum to their maximum values while we did not adjust any other  
441 parameters. To quantify the significance of the input variations, we conducted a t-test (Table A2). For  
442 this, we compared the amount of redistributed sediment of each model run to the first model run.

443

### 444 **3.6 Impact of burrows on surface processes**

445 We estimated burrow density, as a ratio of pixels with predicted burrows to all pixels. Additionally, we  
446 calculated the ratio of pixels which are part of a burrow aggregation to all pixels which include a burrow.  
447 Burrow aggregation describes at least 4 neighboring pixels with predicted burrows. We calculated the  
448 amount of excavated sediment as a sum of burrow density and the burrow excavation rate as estimated  
449 in Grigusova et al. (2022).

450 To estimate the impact of burrows on sediment redistribution and surface runoff, we ran the DMMF  
451 model for the time period from 1<sup>st</sup> April 2016 until 31<sup>th</sup> December 2021 for all hillslope catchments. We  
452 ran the model (i) with no burrows and (ii) with entire burrows. We estimated (i) sediment redistribution  
453 (accumulation - erosion) and (ii) surface runoff. We analyzed the redistribution and runoff on the plot (1  
454 m<sup>2</sup>) and hillslope catchment (1 ha) scale.

455 Lastly, to analyze under which biotic and abiotic environmental parameters (topography, vegetation  
456 cover) the bioturbation enhances sediment erosion or accumulation, we set-up a generalized additive  
457 model (GAM) (Wood, 2006). For this, we first subtracted the output of the model with no burrows from  
458 the output of the model with entire burrows. Within each pixel, two processes are happening  
459 simultaneously: a certain amount of sediment erodes, and a certain amount of sediment accumulates. To  
460 estimate the sediment redistribution for each pixel of each model run, we estimate which of these processes  
461 dominated. Positive pixel values thus mean, bioturbation enhanced sediment accumulation, negative  
462 pixel values mean, bioturbation enhanced sediment erosion. We tested the following environmental  
463 parameters: mound density, vegetation cover, elevation, slope, aspect, TRI, TPI, curvature and  
464 connectivity and wetness index. The model performance was evaluated by the percentage of explained  
465 data variance. We analyzed the impact of environmental parameters within 1-meter and within 10-meter  
466 distance from the burrows.

467

## 468 **4 Results**

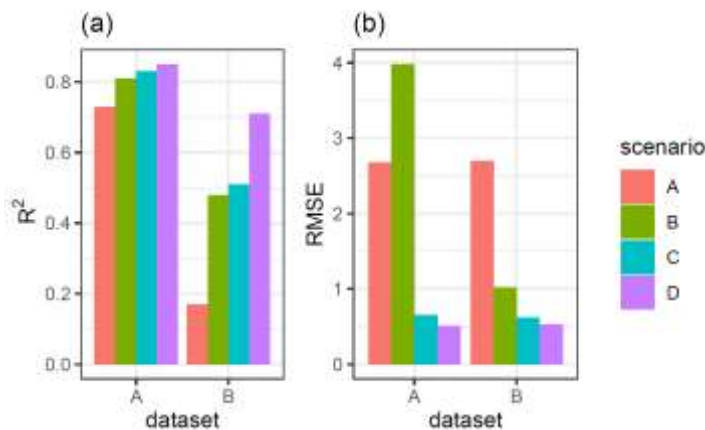
### 469 **4.1 Model sensitivity test and accuracy**



470 Parameters which significantly influenced the model output were precipitation, slope, vegetation cover,  
 471 surface roughness, silt content and water content (Table A2). There was correlation between some of  
 472 the spatial model parameters (Fig. A10), especially between the initial and saturated water content;  
 473 between water content and vegetation cover; and between clay content and field capacity. However, a  
 474 high correlation between spatial parameters does not mean that these parameters impact the sediment  
 475 redistribution in a similar way.

476 We quantified the model performance by comparing the modelled and measured sediment  
 477 redistribution. The performance varied depending on the burrow inclusion (Figure 4 and 5). The  
 478 performance of the model without any bioturbation was lower ( $R^2 = 0.73$ , RMSE = 1.50, MSE = 2.27),  
 479 as when burrow entrances ( $R^2 = 0.81$ , RMSE = 1.34, MSE = 1.16) or mounds ( $R^2 = 0.83$ , RMSE = 1.10,  
 480 MSE = 1.22) were included. The model had the highest performance when entire burrows were included  
 481 ( $R^2 = 0.85$ , RMSE = 1.01, MSE = 1.01). However, as the scatterplots showed, the model performance  
 482 seemed to be determined strongly by one measurement (Fig. 5). For this reason, we calculated the  
 483 metrics without this measurement (Fig. A2). The model without any burrows ( $R^2 = 0.17$ , RMSE = 1.18,  
 484 MSE = 1.39) in this case performed much lower than models with burrows. The model performance  
 485 continuously strongly increased when burrow entrances ( $R^2 = 0.48$ , RMSE = 0.61, MSE = 0.78), or  
 486 mounds ( $R^2 = 0.51$ , RMSE = 0.75, MSE = 0.57) were included. The model with whole burrows reached  
 487 the highest performance ( $R^2 = 0.71$ , RMSE = 0.63, MSE = 0.39). When we compare the modelled  
 488 redistribution to the sediment redistribution estimated using Time-of-Flight cameras in Grigusova et al.  
 489 (2022), the differences appear to be minor ( $R^2 = 0.62$ , RMSE = 0.12, MSE = 0.35).

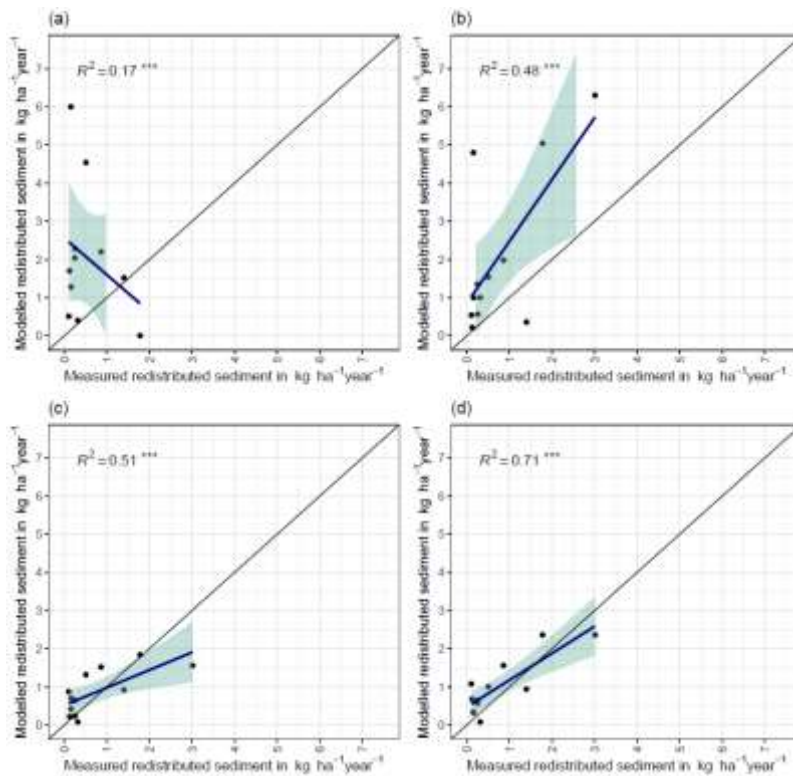
490



491

492 **Figure 4.**  $R^2$  and RMSE of the Morgan-Morgan-Finney soil erosion model. For dataset A, we compared  
 493 the amount of sediment collected in all sediment fences with the modelled eroded sediment (see Fig.  
 494 A3). For dataset B, we removed one measurement, as the  $R^2$  seemed to be defined by this  
 495 measurement (see Fig. A4). For Scenario A, we did not include any burrows into the model. For scenario  
 496 B, we included burrow entrances and for scenario C, we included mounds. For scenario D, we included  
 497 whole burrows into the model. The adjustments made to include entrances, mounds and burrows into  
 498 the model are described in section 3.5.2.

499



500  
501

502 **Figure 5.** Measured and modelled redistributed sediment without an outlier. (a) Model without  
503 bioturbation. (b) Model with entrances. (c) Model with mounds. (d) model with burrows.

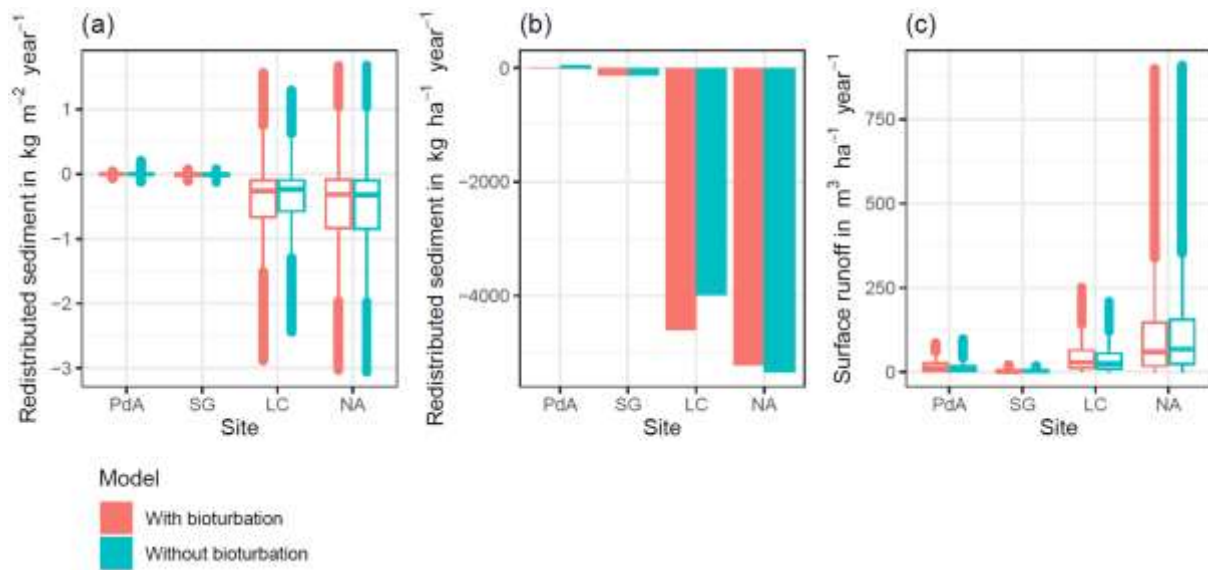
504

#### 505 **4.2 Model output: Surface runoff and sediment redistribution**

506 Hillslope catchment – wide sediment redistribution (1 ha resolution) was the highest in humid NA,  
507 followed by Mediterranean LC, semi-arid SG and arid PdA (Fig. 6a, 6b, 8). In NA, LC and SG, the erosion  
508 processes dominated, while in PdA, more sediment accumulated than eroded. **The impact of burrows  
509 on sediment redistribution was significant in arid PdA, semi-arid SG and Mediterranean LC. Burrows  
510 increased sediment redistribution by 137.8 % ±16.4 % in arid PdA (3.53 kg ha<sup>-1</sup> year<sup>-1</sup> vs. 48.79 kg ha<sup>-1</sup>  
511 year<sup>-1</sup>), by 6.5 % ±0.7 % in semi-arid SG (129.16 kg ha<sup>-1</sup> year<sup>-1</sup> vs. 122.05 kg ha<sup>-1</sup> year<sup>-1</sup>) and by 15.6 %  
512 ±0.3 % in Mediterranean LC (4602.69 kg ha<sup>-1</sup> year<sup>-1</sup> vs. 3980.96 kg ha<sup>-1</sup> year<sup>-1</sup>). Overall, bioturbation  
513 increased sediment accumulation in the arid zone (as the magnitude of the sediment excavation by the  
514 animal exceeded sediment erosion which occurs during rainfall events), but increased sediment erosion  
515 in semi-arid and Mediterranean climate (where animal burrowing activity and rainfall is present). The  
516 largest impact was found under Mediterranean conditions. We found no significant effect on  
517 redistribution in the humid zone (Figure 7). However, impact of bioturbation varied throughout the  
518 hillslope catchment (Figure 7, 8 and 9) – it depended on a specific context if bioturbation supports  
519 sediment erosion or accumulation.**

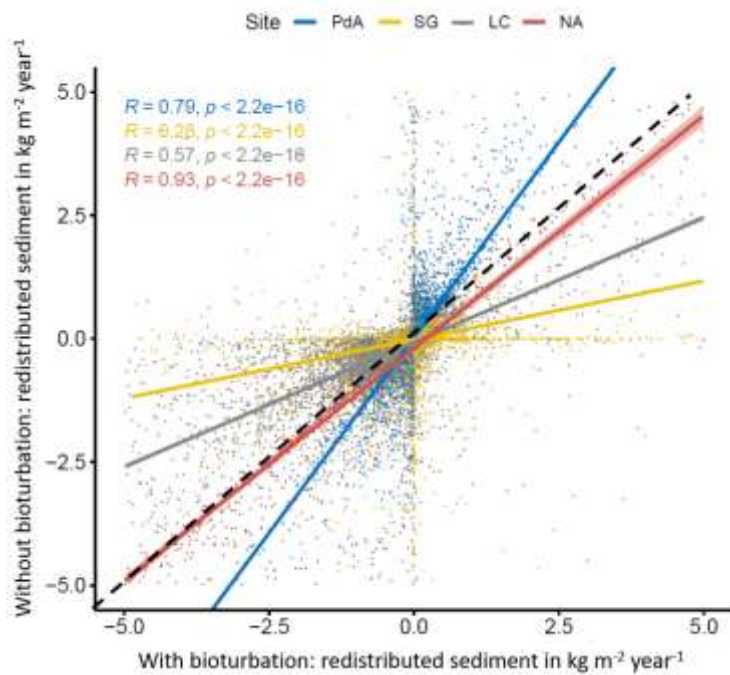
520 Surface runoff was the highest in humid NA, followed by Mediterranean LC, arid PdA and semi-arid SG  
521 (Figure 6c). The impact of burrows on surface runoff was significant in all climate zones. Burrows  
522 increased surface runoff in PdA by 34 %, in SG by 40% and in LC by 4.1 %; and decreased surface  
523 runoff by 5.9 % in NA. Hillslope catchment-wide maps are shown in Fig. A6-A8.

524



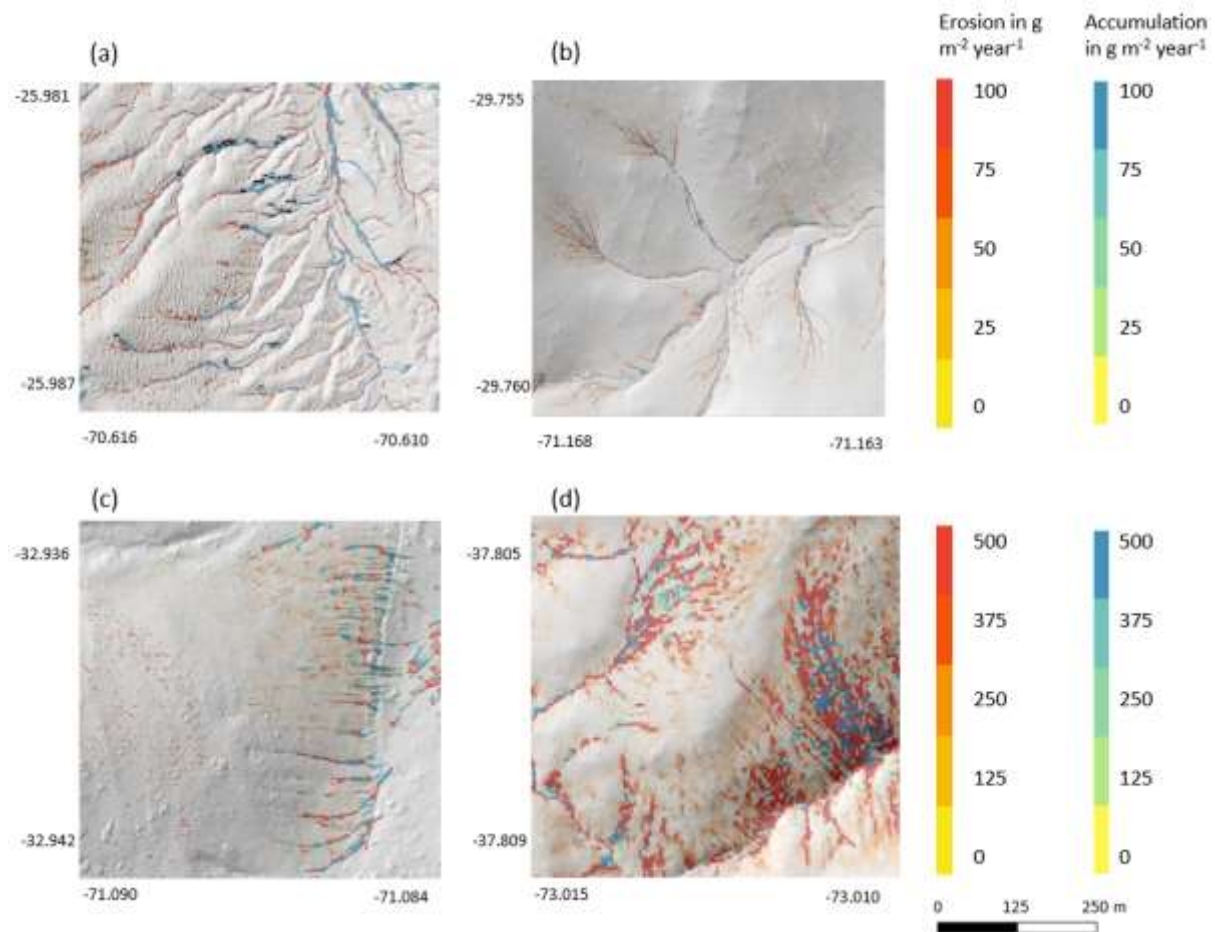
525  
526

527 **Figure 6.** Summary of model outputs across the climate gradient. PdA is arid Pan de Azúcar, SG is  
528 semi-arid Santa Gracia, LC is Mediterranean La Campana, NA is humid Nahuelbuta. Graphs (a) and  
529 (b) show the modelled sediment redistribution. Positive values indicate sediment accumulation; negative  
530 values indicate sediment erosion, in(a) sediment redistribution is shown on a pixel scale in  $\text{kg m}^{-2} \text{ year}^{-1}$ ,  
531 while in(b) sediment redistribution is shown on the hillslope catchment scale in  $\text{kg ha}^{-1} \text{ year}^{-1}$ . The  
532 impact of bioturbation on sediment redistribution was estimated by a t-test and was significant in three  
533 sites: PdA<sup>\*\*\*</sup>, SG<sup>\*\*</sup> and LC<sup>\*\*\*</sup>. Bioturbation increased sediment redistribution by 137.8 % in PdA, by 6.5  
534 % in SG and by 15.6 % in LC. For hillslope catchment-wide maps see Fig. A6-A8. Graph (c) represents  
535 the modelled surface runoff on the hillslope catchment scale in  $\text{m}^3 \text{ ha}^{-1} \text{ year}^{-1}$ . The impact of bioturbation  
536 on surface runoff was estimated by a t-test and was significant at all sites. Bioturbation increased surface  
537 runoff in PdA by 34 %, in SG by 40 % and in LC by 4.1 %; and decreased surface runoff by 5.9 % in  
538 NA. For hillslope catchment-wide maps see Fig. A6.  
539



540  
 541  
 542  
 543  
 544  
 545  
 546  
 547  
 548  
 549  
 550  
 551  
 552  
 553  
 554  
 555

**Figure 7.** Comparison of the model outputs with and without bioturbation of each pixel (0.5 m) in all study sites. The x-axis shows the output of the model with bioturbation, the y-axis the model output without bioturbation. PdA is arid Pan de Azúcar, SG is semi-arid Santa Gracia, LC is Mediterranean La Campana, NA is humid Nahuelbuta. Points represent single pixel values; lines show linear regressions for the sites. The lower R, the higher the impact of burrows on sediment redistribution at the resolution of 0.5 m. The black dashed line symbolizes a perfect correlation – along this line the bioturbation would have no effect on sediment redistribution. Bioturbation lead to more accumulation if the regression line representing results from a particular climate zone is steeper than the perfect correlation line. Bioturbation lead to more erosion if the regression line representing results from a particular climate zone is flatter than the perfect correlation line. Bioturbation increases sediment accumulation in arid PdA (through the high burrowing rate, more sediment is accumulated on the surface than eroded during rainfall events). Bioturbation increases sediment erosion in semi-arid SG and Mediterranean LC. Absolutely, the highest impact on sediment redistribution is in the Mediterranean climate zone. The lowest impact is in the humid zone.



556  
 557 **Figure 8.** Hillslope catchment-wide predicted sediment redistribution. Colours indicate sediment  
 558 redistribution. Grey shadows indicate the hill shading calculated from LiDAR data. (a) Pan de Azúcar,  
 559 (b) Santa Gracia, (c) La Campana, (d) Nahuelbuta.

560

#### 561 **4.3 Role of continuous burrowing activity on sediment redistribution**

562 We included the excavation of the sediment by the animal itself into the model. The density of burrows  
 563 was the highest in arid PdA, then Mediterranean LC, semi-arid SG and the lowest in humid NA. Burrows  
 564 were mostly distributed within groups of several burrows in Mediterranean LC and semi-arid SG, while  
 565 they were more evenly distributed in arid PdA and humid NA. The burrows were of largest size in  
 566 Mediterranean LC, followed by arid PdA, semi-arid SG and humid NA. Similarly, the highest volume of  
 567 excavated sediment at the beginning of the modelling period was in Mediterranean LC and arid PdA.  
 568 The volume of excavated sediment during the burrow reconstruction after rainfall events was the highest  
 569 in humid NA, followed by Mediterranean LC, semi-arid SG and arid PdA. The percentage of sediment  
 570 excavated by the animal to sediment redistributed during rainfall events was 128 % in PdA, 24 % in SG,  
 571 33.5 % in LC and 5.6 % in NA.

572

573 **Table 2.** Impact of animal bioturbation activity on overall sediment redistribution on various scales. The  
 574 bioturbation activity was estimated using Time-of-Flight based cameras in Grigusova et al. 2022. This  
 575 study showed that animals reconstruct their burrows after each rainfall events. During this process, 10  
 576 % of the overall sediment burrow volume is relocated from within the burrow to the surface. We



577 integrated this process into our model and calculated the percentage of newly excavated sediment by  
 578 the animals to the amount of sediment which was redistributed during rainfalls for the period of one year.

Parameter	Units	PdA	SG	LC	NA
Burrow density	ha <sup>-1</sup>	91.35	71.50	84.36	13.30
Burrow aggregations	%	24	62	73	5
Burrow size	m <sup>3</sup>	0.015	0.012	0.047	0.008
Sediment at the surface at the start of modelling	m <sup>3</sup> ha <sup>-1</sup>	1.35	0.88	4.11	0.10
Sediment excavated after each rainfall	m <sup>3</sup> ha <sup>-1</sup>	0.07	0.04	0.22	0.01
Number of rainfall events	year <sup>-1</sup>	3	7	16	137
Sediment excavated by the animal after the rain	m <sup>3</sup> ha <sup>-1</sup> year <sup>-1</sup>	0.21	0.28	3.52	0.69
Sediment redistributed due to rainfall	m <sup>3</sup> ha <sup>-1</sup> year <sup>-1</sup>	0.44	1.17	10.51	12.21
Excavated sediment to redistributed sediment	%	47	24	33.5	5.6

579

#### 580 4.4 Role of adjacent environment

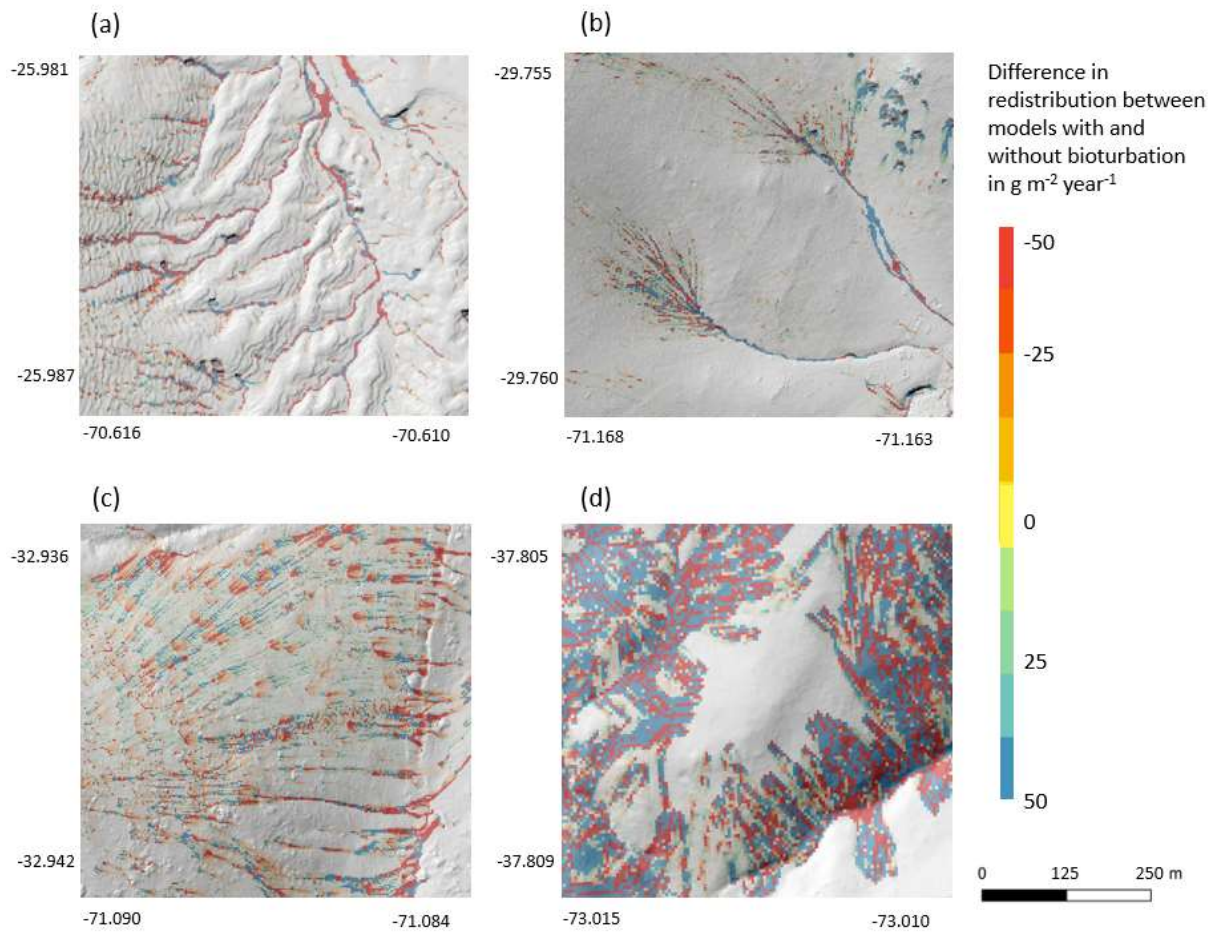
581 We subtracted the output of the model with included burrows from the output of the model without  
 582 burrows (Figure A8). Although, the burrows on average enhanced sediment erosion on the hillslope  
 583 catchment – scale, the high-resolution maps unveiled that burrows enhance sediment erosion within  
 584 some pixels while they rather increased sediment accumulation within others.

585 The amount of data variance explained by the GAM models (see section 3.6.) differed between models  
 586 (Table A3). Models estimating the impact of environmental parameters on sediment redistribution within  
 587 1-meter distance from the burrows, explained 3.84 % of variance in PdA, 37.1 % in SG, 46 % in LC and  
 588 42. % in NA. Models estimating the impact of environmental parameters on sediment redistribution  
 589 within 10-meter distance from the burrows, explained 1.99 % of variance in PdA, 12.8 % in SG, 52 % in  
 590 LC and 72.9 % in NA. The parameters selected for SG were slope, roughness, curvature, TRI and NDVI.  
 591 Parameters selected for LC were elevation, slope, NDVI, sinks and roughness. Parameters selected for  
 592 NA were elevation, slope, aspect, TRI, sinks and roughness (Figure 10).

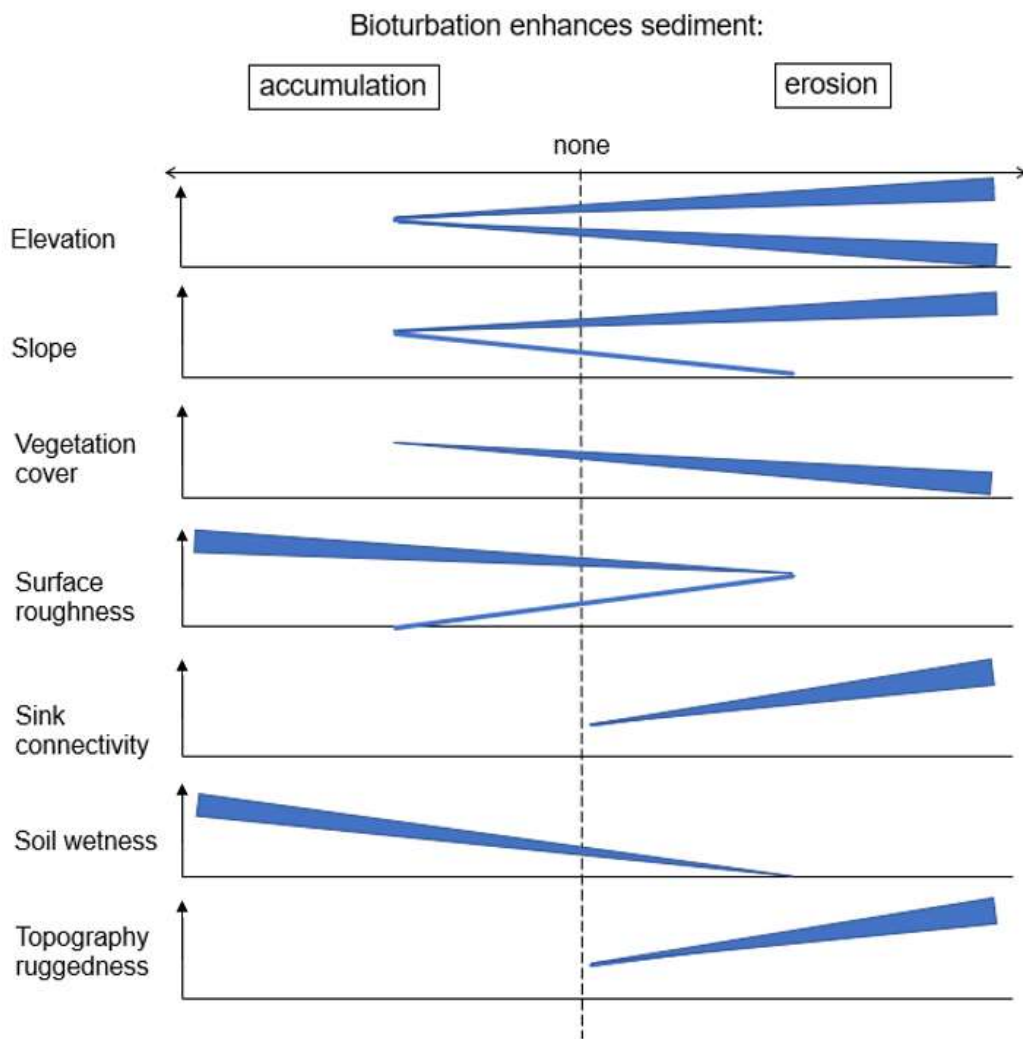
593 Bioturbation strongly increased sediment redistribution (erosion and accumulation) at high values of  
 594 elevation, slope, surface roughness TRI, sinks and topographic wetness index, at the middle values of  
 595 elevation and aspect, and at low values of profile curvature and NDVI. From these parameters,  
 596 bioturbation increased sediment erosion at high and middle values of elevation, at high values of slope,  
 597 sinks and TRI, and at low values of profile curvature. Bioturbation increased sediment accumulation at  
 598 high values of surface roughness and topographic wetness index and at low values of NDVI (Fig. A3 –  
 599 A8).

600 Bioturbation somewhat enhanced sediment erosion at medium values of surface roughness, NDVI and  
 601 sinks, and at low values of topographic wetness index. Bioturbation somewhat increased sediment  
 602 accumulation at low values of slope and TRI, at low and medium values of elevation and at high values  
 603 of profile curvature.

604



605  
 606 **Figure 9.** Hillslope catchment-wide impact of bioturbation on sediment redistribution. Colour indicates  
 607 the impact. Positive values indicate bioturbation enhanced sediment accumulation, negative values  
 608 indicate bioturbation enhanced sediment erosion. Grey shadows indicate the hill shading calculated  
 609 from LIDAR data. (a) Pan de Azúcar, (b) Santa Gracia, (c) La Campana, (d) Nahuelbuta.  
 610



611  
 612 **Figure 10.** This figure is a conceptual summary of the detailed results from figures A3 – A8. Bioturbation  
 613 increases erosion or accumulation depending on the values of environmental parameters. The  
 614 dependencies are the same for all climate zones. The figure is the conceptual summary for all climate  
 615 zones, therefore, there are no values stated on the x- and y-axes. The x-axis shows if bioturbation  
 616 increases erosion or accumulation. The y-axis are environmental parameters. Line thicknesses indicate  
 617 the magnitude of impact. Please note that bioturbation has no impact on sediment redistribution in  
 618 regions with low sink connectivity and topographic ruggedness. The relationship between the values of  
 619 environmental parameters and the impact of bioturbation is not linear: Bioturbation can have the same  
 620 impact on sediment redistribution at high or low values of an environmental parameter, but a contrasting  
 621 impact at middle values of this parameter (as in this case for elevation, slope or surface roughness).

622  
 623 **5. Discussion**

624 **5.1 The inclusion of bioturbation increases model performance**

625 Overall, our DMMF model including bioturbation performed much better than the model without  
 626 bioturbation. The DMMF model without bioturbation performed worse (RMSE of  $1.18 \text{ kg ha}^{-1} \text{ year}^{-1}$  and  
 627  $R^2$  of 0.17) than the model with bioturbation (RMSE was  $0.63 \text{ kg ha}^{-1} \text{ year}^{-1}$  and  $R^2$  was 0.71).

628 We hence argue that the higher accuracy of our model can be explained with the inclusion of  
 629 bioturbation. This is confirmed by the fact that our model run without bioturbation performed similarly to

630 previously run models without bioturbation: In earlier studies, the accuracy of the MMF model reached  
631 an RMSE in between 4.9 and 8.2 kg ha<sup>-1</sup> year<sup>-1</sup>, with an estimated R<sup>2</sup> of in between 0.21 and 0.57 (Jong  
632 et al., 1999; Vigiak et al., 2005; López-Vicente et al., 2008; Vieira et al., 2014; Choi et al., 2017).  
633 However, we acknowledge that previous studies were all conducted in more temperate climate zones.  
634 To be able to compare our results with previous studies, we calculated the model performance  
635 considering solely the Mediterranean and humid climate zone, which are more similar in climate to the  
636 more temperate locations of previous studies. The performance of the model was still high (R<sup>2</sup> = 0.72,  
637 RMSE = 0.45 kg ha<sup>-1</sup> year<sup>-1</sup>), confirming the conclusion that bioturbation increased model performance.  
638 We compared the modelled impact of bioturbation on sediment redistribution with the impact of  
639 bioturbation estimated in previous studies. In the humid zone, our model predicted an erosion up to 3.5  
640 kg m<sup>-2</sup> year<sup>-1</sup>. This estimation is in line with erosion rates established by in-situ measurements in other  
641 studies conducted in a more humid climate zone (between 1.5 kg m<sup>-2</sup> year<sup>-1</sup> and 3.7 kg m<sup>-2</sup> year<sup>-1</sup>) (Black  
642 and Montgomery, 1991; Yoo and Mudd, 2008; Yoo et al., 2005; Rutin, 1996). This also confirms the  
643 reliability of our approach. Previous authors estimated the impacts using rainfall simulators, erosion pins  
644 or splash boards. The measurements were conducted for a time period between 3 months and 3 years  
645 and the sites were revisited for each estimation. We do not compare our results with studies which  
646 previously applied models to estimate impacts of bioturbation, as, to our knowledge, none of the  
647 previous studies integrated vertebrate burrow structures into a soil erosion model and ran the model on  
648 a daily basis.

649

## 650 **5.2 The relevance of bioturbation for sediment redistribution depends on the environmental** 651 **context**

652 On the hillslope catchment scale (1 ha), our study finds that bioturbation increases erosion in semi-arid  
653 and Mediterranean zone, accumulation in the arid zone and has no impact within the humid zone (Figure  
654 6b). In contrast, bioturbation increases both, erosion, and accumulation, on the plot scale (1 m<sup>2</sup>) (Figure  
655 6a). On this scale, in the arid and semi-arid zone, sediment erosion and accumulation were predicted to  
656 be about equal (erosion and accumulation both up to 0.1 kg m<sup>-2</sup> year<sup>-1</sup> in the arid zone, and erosion and  
657 accumulation both up to 0.2 kg m<sup>-2</sup> year<sup>-1</sup> in the semi-arid zone (see Figure 6a)). Bioturbation marginally  
658 increased erosion and decreased accumulation in the semi-arid zone but reduced by twofold  
659 accumulation in the arid zone. In contrast, in the Mediterranean and humid zone, erosion was predicted  
660 to be almost double when compared to accumulation (predicted erosion up to 2.5 kg m<sup>-2</sup> year<sup>-1</sup>, and  
661 accumulation up to 1.4 kg m<sup>-2</sup> year<sup>-1</sup>). Inclusion of bioturbation increased erosion up to 3 kg m<sup>-2</sup> year<sup>-1</sup>,  
662 and accumulation up to 1.6 kg m<sup>-2</sup> year<sup>-1</sup> in the Mediterranean zone, while it had no significant effect in  
663 the humid zone. We argue that sediment redistribution due to bioturbation is heavily influenced by meso-  
664 topographic structures which determine the flow path of surface runoff and influence the infiltration  
665 processes. Due to this, the erosion and accumulation on the plots scale is heavier impacted by  
666 bioturbation with increasing surface runoff.

667 Our study found an increase of erosion in the semi-arid and Mediterranean climate zone to be between  
668 6.5 % and 15.6 % due to bioturbation. Previous studies found that already a small increase of erosion  
669 has significant impacts on the whole hillslope catchment. A 10% increase in erosion rates over a 10-

670 year period can lead to significant changes in the landscape, including e.g. a 20-30% reduction in soil  
671 thickness and an increase in sediment transport in nearby rivers (Kuhn 2016).

672 According to our analysis, bioturbation increases erosion or accumulation of sediment mostly based on  
673 an interplay between topographic structures elevation, slope and TRI (Figure 10). Over all research  
674 sites, this study found that bioturbation leads to an increase in surface erosion in areas where erosional  
675 processes dominate (upper, and/or steeper slopes), and tends to increase sediment accumulation in  
676 areas where sediment is naturally deposited, e.g. lower slopes or shallow depressions (Figure 10). This  
677 finding is based on the fact that erosion in general is positively affected by slope, and negatively by  
678 surface roughness and vegetation (Rodríguez-Caballero et al., 2012; Wang et al., 2013; Kirols et al.,  
679 2015). Additionally, the redistribution of sediment is largely affected by topographic meso-/macroforms,  
680 such as rills or cliffs. These can be quantified by topographic ruggedness index (TRI) which describes  
681 the amount of elevation drop between adjacent cells of DEM (Wilson et al., 2007). At high values of this  
682 index, we would therefore expect high erosion rate, due to concentrated runoff within the connected rills  
683 or undisturbed flow of runoff from the cliffs downslope.

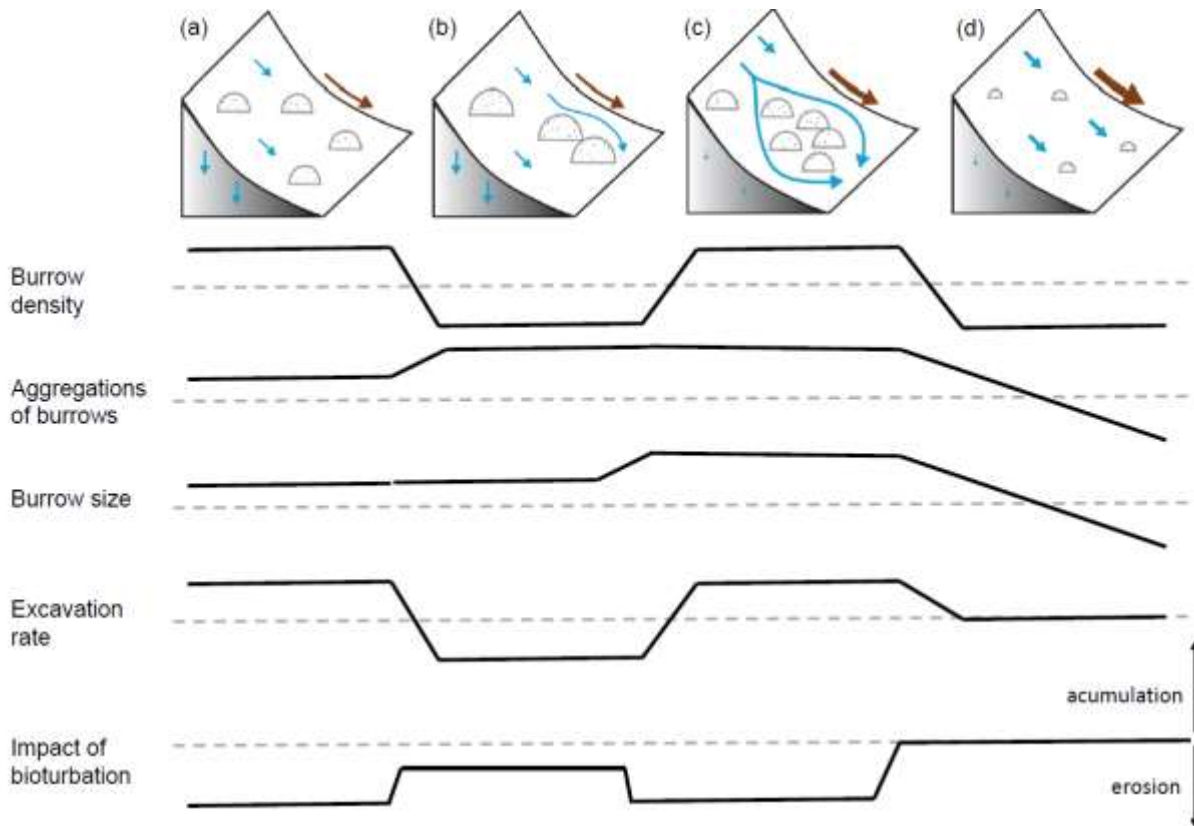
684 Our data show that one burrow provides up to 0.43 m<sup>3</sup> of additional loose sediment at the surface (Table  
685 2), while the surface roughness increases up to 200 % (Grigusova et al., 2022). When including burrows  
686 into the model, at the slope values from 0 to 5 degrees, the presence of burrows had no impact on  
687 sediment redistribution. From 5 degrees onwards it increased sediment erosion proportionally to the  
688 slope of the hillside (an increased erosion from 0.4 g ha<sup>-1</sup> year<sup>-1</sup> in the semi-arid zone until up to 150 kg  
689 ha<sup>-1</sup> year<sup>-1</sup> in the Mediterranean zone, Fig. A3 – A6). Similarly, at locations with elevation drops ranging  
690 from 0 m until 0.2 m (lower TRI values), the presence of burrows had no impact. However, at locations  
691 with elevation drops of 0.2 until 0.5 m (higher TRI values), bioturbation increases sediment erosion by  
692 1.5 kg ha<sup>-1</sup> year<sup>-1</sup> (Fig. A3 – A8). Lastly, bioturbation proportionally increased accumulation when the  
693 surface roughness values were above 0.5 (an increased accumulation from 0.2 g ha<sup>-1</sup> year<sup>-1</sup> in semi-arid  
694 zone until 5000 kg ha<sup>-1</sup> year<sup>-1</sup> in the Mediterranean zone, Fig. A3 – A6).

695 We conclude that in locations with slope values over 5 degrees, or at locations with sudden drops in  
696 elevation (high TRI), and connected rills, more sediment is eroding than accumulating. Here, additional  
697 surface sediments generated by bioturbators provides more source material for erosion and thus  
698 bioturbation increases sediment erosion at these locations (Figure 10 and 11). In contrast, at locations  
699 with a slope below 5 degrees, where processes are dominantly controlled by surface roughness,  
700 sediment accumulation caused by bioturbation increases proportionally when the surface roughness  
701 has a value above 0.5. This is likely because burrows through their above-ground structures heavily  
702 increase surface roughness (Grigusova et al., 2022), and hence the presence of bioturbating animals  
703 leads to an increase in sediment accumulation.

704 Additionally, we hypothesize that it is not only the additional availability of sediment on the surface and  
705 the topography of the vicinity which controls the contribution of bioturbation to sediment surface flux, but  
706 also the spatial distribution of animal burrows. We interpret that in locations with high burrow  
707 aggregation, surface flow might be redirected and centralized around the aggregates and thus increase  
708 sediment erosion in the areas adjacent burrow aggregates (Figure 11). This mechanism could explain  
709 why bioturbation promotes sediment erosion especially in the Mediterranean zone where burrows are



710 more aggregated. The relative role of burrow aggregation should be studied in detail and included in  
 711 future studies.  
 712



713  
 714 **Figure 11.** Context dependency of sediment redistribution. (a) Pan de Azúcar, (b) Santa Gracia, (c) La  
 715 Campana, and (d) Nahuelbuta. Brown arrows indicate the direction and magnitude of overall sediment  
 716 redistribution within each climate zone. Blue arrows indicate the direction of flow (runoff vs. infiltration).  
 717 Half-moons indicate the distribution and size of the burrows.

718  
 719  
 720 **6. Conclusion**

721 Our study found that the inclusion of vertebrate bioturbators' burrows into a soil erosion model  
 722 significantly increases its reliability. Vertebrate bioturbators increase sediment accumulation in the arid  
 723 climate zone, sediment erosion in the semi-arid and Mediterranean zone and have no impact on  
 724 sediment redistribution in the humid. Our study furthermore shows that the impact of bioturbation heavily  
 725 depends on the adjacent environmental parameters. The burrows increase sediment erosion at high  
 726 and low values of elevation, at high values of slope, sink connectivity and topography ruggedness, and  
 727 at low values of vegetation cover. The burrows increase accumulation at high values of surface  
 728 roughness and soil wetness. This means that overall, on geological time scales, as burrowing animals  
 729 increase both, erosion in steeper zones, and accumulation in areas with gentler slopes and higher  
 730 roughness, hillslope relief should become faster equalised and overall, more flat. This tendency is most  
 731 pronounced in the Mediterranean zone with high burrow density and excavation rates, as well as  
 732 comparably high precipitation rates.

733  
734 **Funding:** This study was funded by the German Research Foundation, DFG [grant numbers  
735 BE1780/52-1, LA3521/1-1, FA 925/12-1, BR 1293-18-1], and is part of the DFG Priority Programme  
736 SPP 1803: EarthShape: Earth Surface Shaping by Biota, sub-project “Effects of bioturbation on rates  
737 of vertical and horizontal sediment and nutrient fluxes”.

738 **Institutional Review Board Statement:** Not applicable.

739 **Informed Consent Statement:** Not applicable.

740 **Acknowledgments:** We thank CONAF for the kind support provided during our field campaign.

741 **Competing interests:** There is no conflict of interest.

742 **Author contribution:** PG set up the model, analysed the data and wrote the manuscript draft; PG and  
743 AL performed the measurements AL, JB, NF, RB, DK, PP, LP, CdR reviewed and edited the manuscript.

744 **Code/Data availability:** The estimated soil properties (DOI: [10.5678/wsrb-9f70](https://doi.org/10.5678/wsrb-9f70)), modelled sediment  
745 redistribution (DOI: [10.5678/32wa-d179](https://doi.org/10.5678/32wa-d179)) and model code ([https://gitlab.uni-marburg.de/fb19/ag-  
746 bendix/model-sediment-redistribution-caused-by-bioturbating-animals](https://gitlab.uni-marburg.de/fb19/ag-bendix/model-sediment-redistribution-caused-by-bioturbating-animals)) was published via LCRS data  
747 services.

748 **Special Issue statement:** I would like to stress that the submission should be part of the Copernicus  
749 special Issue (Earth surface shaping by biota (ESurf/BG/ESD/ESSD/SOIL inter-journal SI) initiated by  
750 the EarthShape consortium.

751

752

753 burrows. The dashed line indicates the median value of each parameter for the first four parameters.

754

## 755 **Supplementary material**

756 **Table A1:** R<sup>2</sup> and RMSE of random forest models trained for the prediction of soil properties needed for  
757 model parametrization. RMSE is root mean square error.

Variable	R <sup>2</sup>	RMSE
Soil water content	0.80	0.05
Bulk density	0.60	0.22
Porosity	0.63	0.09
Silt	0.64	0.04
Middle silt	0.64	0.04
Sand	0.68	0.09
Middle sand	0.64	0.05
Organic components	0.77	0.05
Organic carbon	0.70	0.03

758

759 **Table A2.** Model sensitivity analysis. For the analysis, the minimum, maximum and mean value of each  
760 parameter was calculated. The model was run for a hillslope catchment of 1km<sup>2</sup> with homogenous mean  
761 parameters. Then, the minimum and maximum values of each parameter were tested. Each parameter  
762 was stepwise changed to its minimum or maximum value while the remaining parameters stayed  
763 homogenous. The significance of the parameter was estimated by a t-test conducted between the

764 erosion estimated by the model with homogenous mean parameters and the erosion estimated by the  
 765 model with varying minimum and maximum parameter values. Only significant parameters are shown.

Parameter	mean value	min value	max value	mean erosion [kg m <sup>-1</sup> ]	Min erosion [kg m <sup>-1</sup> ]	Max erosion [kg m <sup>-1</sup> ]	Erosion [kg m <sup>-1</sup> ]
Precipitation [mm rainfall event <sup>-1</sup> ]	19.9	0.2	65.6	0.07	0	4.1	
clay content [%]	10.61	3.87	34.64	0.07	0.07	0.07	
silt content [%]	38.49	13.32	59.59	0.07	0.04	0.11	
sand content [%]	47.04	24.13	79.17	0.07	0.07	0.07	
water content [%]	3.87	2.38	12.68	0.07	0.09	0.06	
roughness [-]	0.97	0	236.8	0.07	0.34	0.01	
vegetation [%]	79.54	50.38	92.48	0.07	0.01	0.004	
Slope of DEM [°]	18.2	0	89.78	0.07	0	inf.	

766  
767

768 **Table A3.** Summary of GAM models. We analyzed the impact of parameters within a 1-meter and 10-  
 769 meter distance from burrows. The Stars indicate p-values of the selected parameters. p\*\*\* < 0.001, p\*\*  
 770 < 0.01, p\* < 0.05, p. < 0.1. One GAM model was run per parameter. Only results for models with an  
 771 explained variance above 5 % are shown.

Parameters	Within 1 meter from burrows				Within 10 meters from burrows			
	PdA	SG	LC	NA	PdA	SG	LC	NA
Explained Variance	3.8 %	37 %	46 %	42 %	2.0 %	13 %	52 %	73 %
Burrow density	.				.			
Elevation			***	***	*		*	***
Slope		***					*	**
Aspect	.	**		*	*			.
Roughness		***					**	*

TPI								
TRI		**		**				
Plan curvature		.						.
Profile curv.		**	.					
NDVI			**			**		.
Sinks			*	***	*		*	
Wetness				**				
Flow direction								
Flow path								
Catchment		*			*			
Catchment slope		***		.				

772

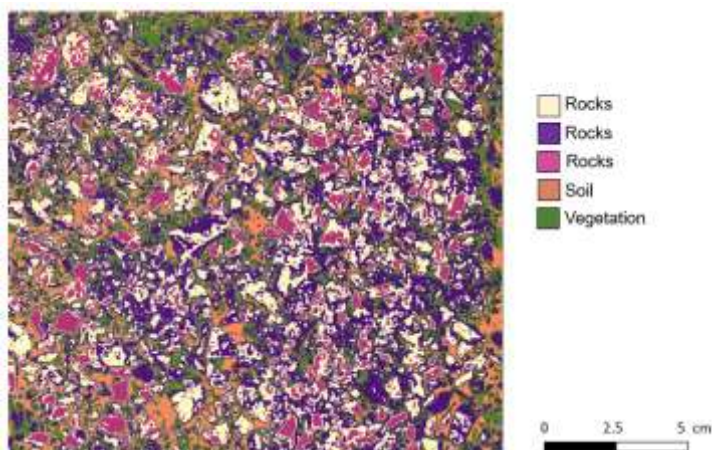
773 **Table A4.** Review of studies which integrated any kind of bioturbation into models. Previous models  
774 integrated either benthic, invertebrate or single species of vertebrate bioturbators. Models applied  
775 either described the vertical soil mixing or long-term landscape evolution models. None of the previous  
776 studies included vertebrate burrows of bioturbators into an erosion model which would be capable to  
777 capture the daily redistribution processes.

References	Bioturbators	Integrated processes	Targeted process	Model
Francois et al. 1997, Francois et al. 2002, Kadko and Heath 1984, Croix et al. 2002 and several others	Various benthic bioturbators	Equations describing soil mixing within a floodplain	Vertical soil mixing within a floodplain	Mathematical equations
Orvain et al. 2006, Román – Sánchez et al. 2019, Orvain 2005, Orvain 2003, Sanford 2008 and several others	Various invertebrates	Equations describing vertical soil mixing	Influence of vertical soil mixing on lateral redistribution	Mathematical equations
Gabet 2000	Pocket gophers	Equation describing diffusion caused by gopher bioturbation	Relief changes over 40 000 years, lateral redistribution	Landscape evolution
Gabet et al. 2014	Pocket gophers	Equations describing sediment accumulation caused by gophers	Relocation of sediment to create Mima mounds	Landscape evolution
Temme and Vanwallegem 2016	Not specified invertebrates	Bioturbation causes soil mixing between model layers. Mixing	Soil and landscape evolution	Landscape evolution

Vanwallegem et al. 2013		is proportional to depth in the profile, soil thickness, and soil carbon content, and layer distance		Landscape evolution
Yoo and Mudd 2008		Bioturbation is considered as the cause of colluvial transport. Colluvial fluxes are calculated as a function of soil thickness and slope gradient on sloping grounds		Landscape evolution
Pelletier et al. 2013		Vertical soil mixing. Rate increases linearly with aboveground biomass.	creep including abiotic and bioturbation-driven transport	Landscape evolution
Van der Meij et al. 2020		Vertical soil mixing. Rate depends on vegetation type.	Soil and landscape evolution	Landscape evolution
Our model	Vertebrates	The model includes burrow structure, adjusted soil properties and adjusted vegetation cover. Burrow distribution determined by machine learning.	Daily lateral sediment redistribution	Daily erosion model

778

779



780

781 **Figure A1.** Example of the unsupervised k-means classification of the surface photo from La Campana.

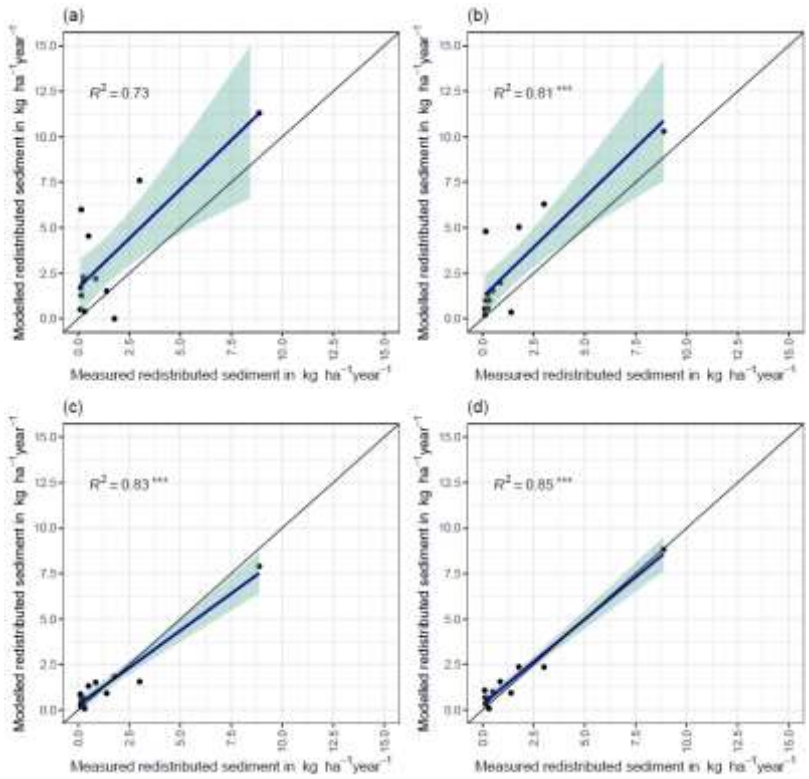
782 Original photo was taken by Paulina Grigusova. The collection of in-situ data is explained in section 3.1.,

783 the estimation of soil properties in section 3.2. The image was classified into 5 classes using

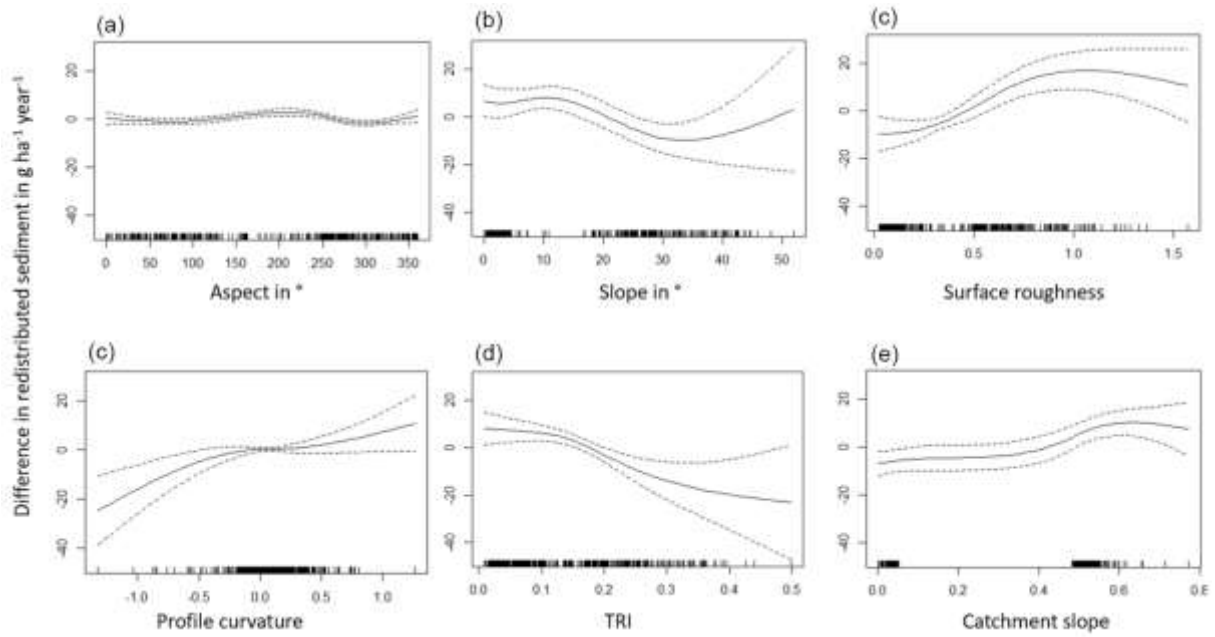
784 unsupervised k-means classification; the land cover was then assigned manually. In some cases, like



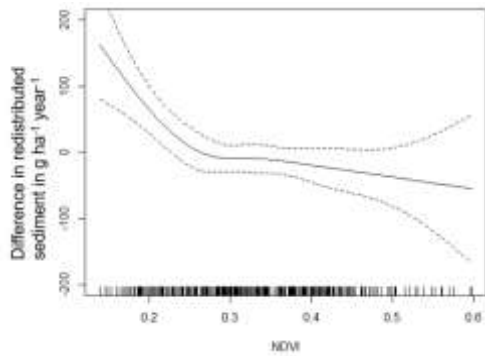
785 in this case for rocks, multiple k-means classes stand for the same land cover. These were then unified  
786 to the class "rocks".  
787  
788



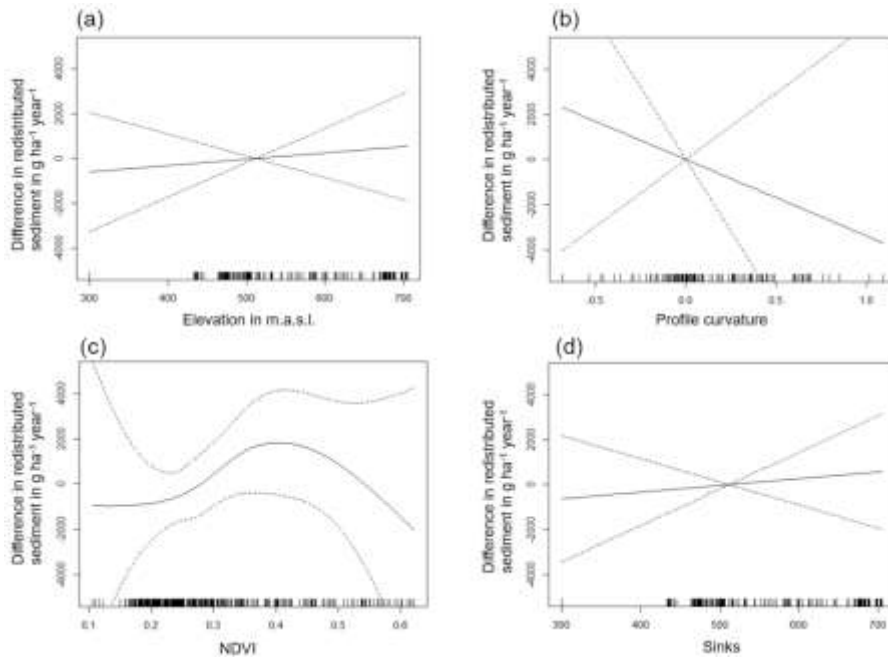
789  
790 **Figure A2.** Measured and modelled redistributed sediment for different scenarios. (a) Model without  
791 bioturbation. (b) Model with entrances. (c) Model with mounds. (d) model with burrows.  
792  
793  
794  
795  
796



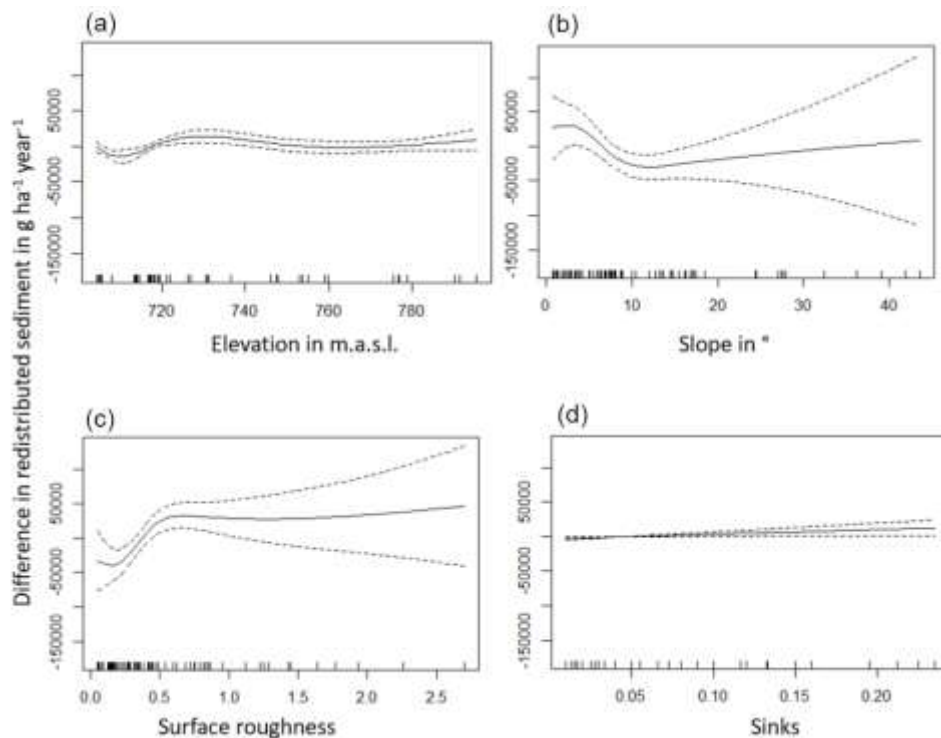
797  
 798 **Figure A3.** Environmental parameters influencing impact of bioturbation on sediment redistribution in  
 799 Santa Gracia within 1-meter distance from burrows. Positive values indicate bioturbation enhances  
 800 sediment accumulation at the respective parameter values, negative values indicate bioturbation  
 801 enhances sediment erosion at the respective parameter values.  
 802



803  
 804 **Figure A4.** Environmental parameters influencing impact of bioturbation on sediment redistribution in  
 805 Santa Gracia within 10-meter distance from burrows. Positive values indicate bioturbation enhances  
 806 sediment accumulation at the respective parameter values, negative values indicate bioturbation  
 807 enhances sediment erosion at the respective parameter values.  
 808  
 809

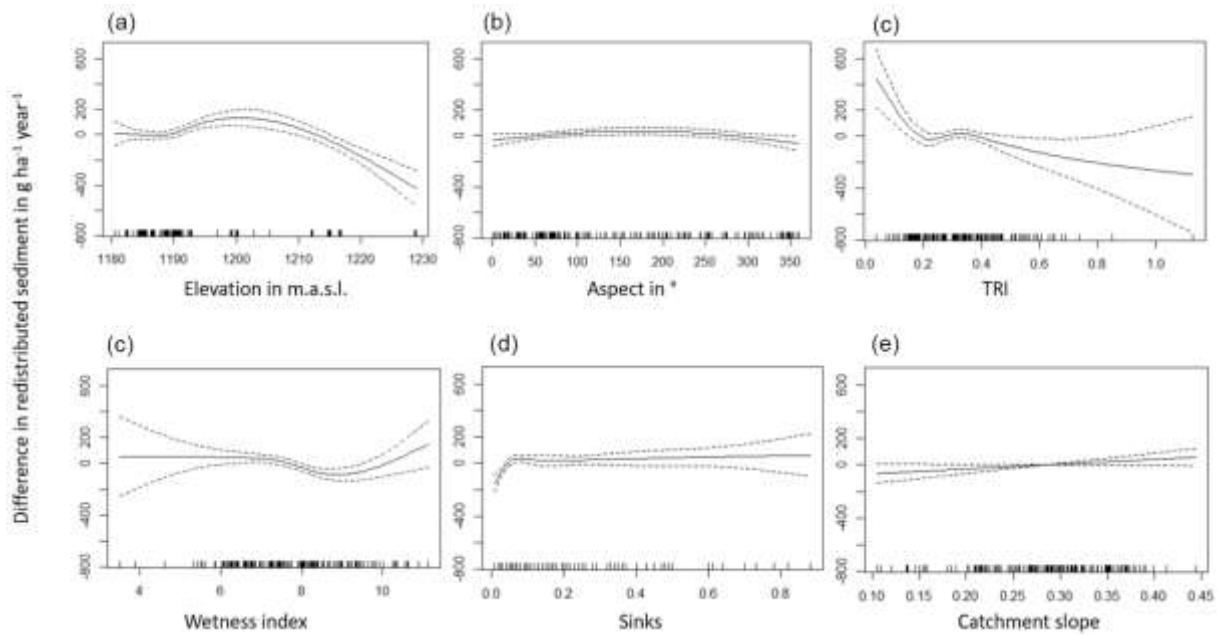


810  
 811 **Figure A5.** Environmental parameters influencing impact of bioturbation on sediment redistribution in  
 812 La Campana within 1-meter distance from burrows. Positive values indicate bioturbation enhances  
 813 sediment accumulation at the respective parameter values, negative values indicate bioturbation  
 814 enhances sediment erosion at the respective parameter values.  
 815



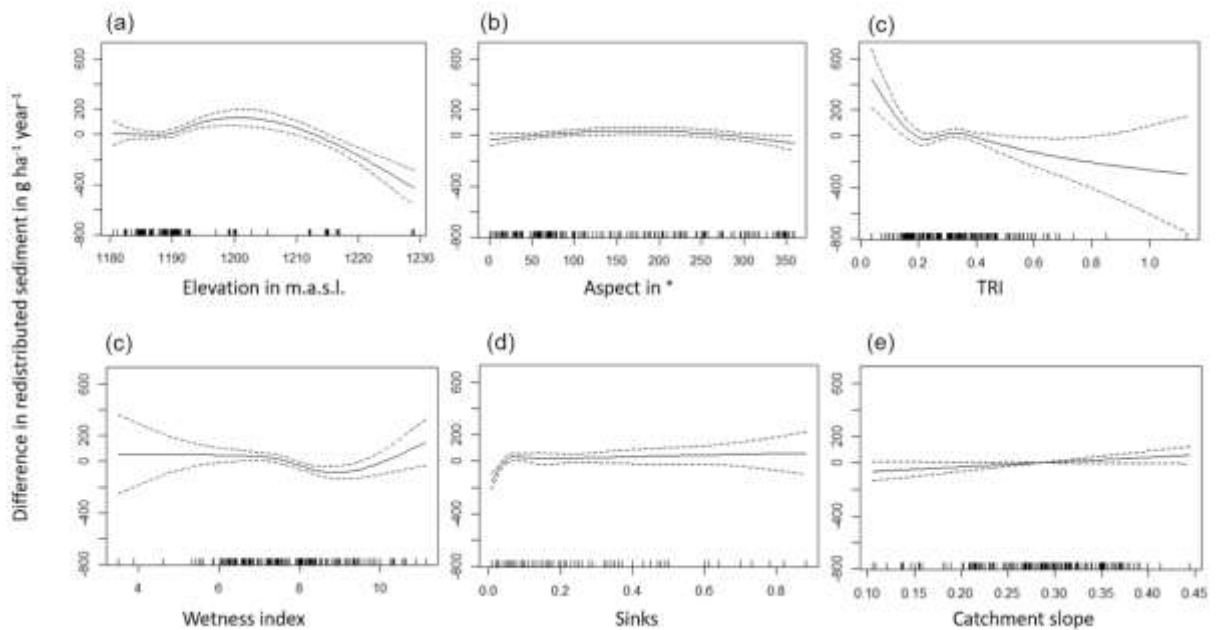
816  
 817 **Figure A6.** Environmental parameters influencing impact of bioturbation on sediment redistribution in  
 818 La Campana within 10-meter distance from burrows. Positive values indicate bioturbation enhances  
 819 sediment accumulation at the respective parameter values, negative values indicate bioturbation  
 820 enhances sediment erosion at the respective parameter values.  
 821

822



823

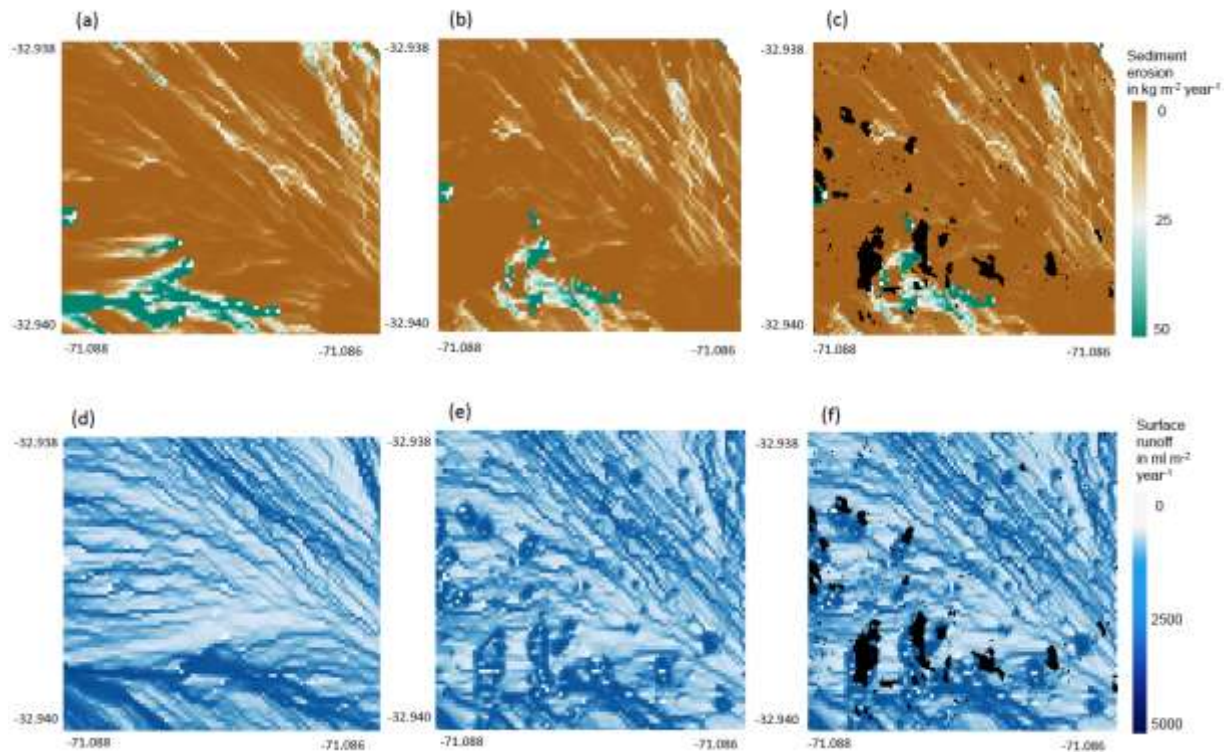
824 **Figure A7.** Environmental parameters influencing impact of bioturbation on sediment redistribution in  
825 Nahuelbuta 1-meter distance from burrows. Positive values indicate bioturbation enhances sediment  
826 accumulation at the respective parameter values, negative values indicate bioturbation enhances  
827 sediment erosion at the respective parameter values.



828

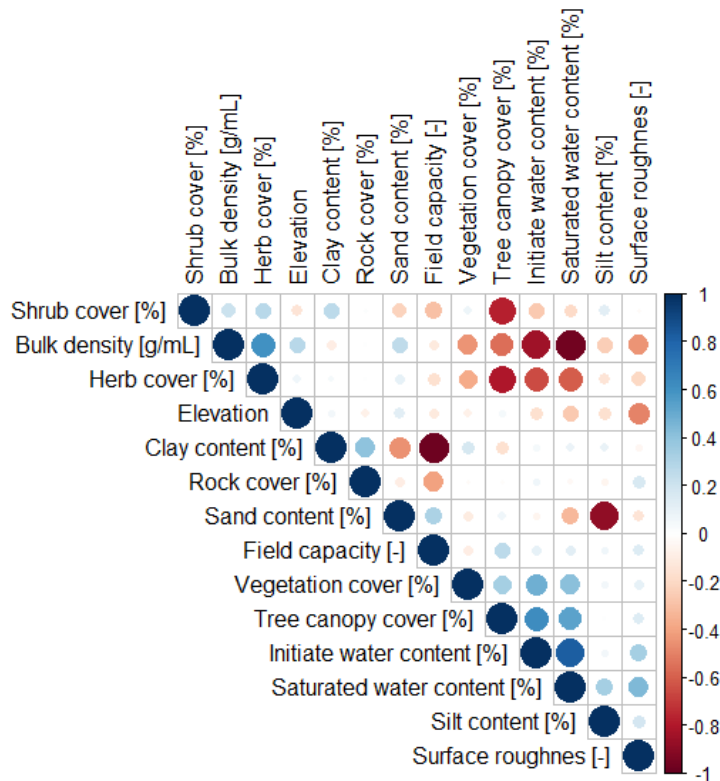
829 **Figure A8.** Environmental parameters influencing impact of bioturbation on sediment redistribution in  
830 Nahuelbuta 10-meter distance from burrows. Positive values indicate bioturbation enhances sediment  
831 accumulation at the respective parameter values, negative values indicate bioturbation enhances  
832 sediment erosion at the respective parameter values.

833



834  
 835 **Figure A9.** Burrow aggregation concentrates the runoff and increases erosion. Example for the north-  
 836 facing hillside in Mediterranean La Campana for the time period of one year. (a) Sediment erosion as  
 837 estimated by model without bioturbation. (b) Sediment erosion as estimated by model with bioturbation.  
 838 (c) Sediment erosion as estimated by model with bioturbation with predicted burrow locations. (d)  
 839 Surface runoff as estimated by model without bioturbation. (e) Surface runoff as estimated by model  
 840 with bioturbation. (f) Surface runoff as estimated by model including bioturbation and predicted burrow  
 841 locations. Black colour indicates, at least one burrow was located within this pixel. Four neighbouring  
 842 pixels which contain a burrow form a burrow aggregation.  
 843





844  
845  
846  
847

**Figure A10.** Correlation matrix between the model input parameters.

## 848 References

849 Anderson, R. S., Rajaram, H., and Anderson, S. P.: Climate driven coevolution of weathering profiles and  
850 hillslope topography generates dramatic differences in critical zone architecture, *Hydrol. Process.*, 33, 4–19,  
851 <https://doi.org/10.1002/hyp.13307>, 2019.

852 Beasley, D. B., Huggins, L. F., and Monke, E. J.: ANSWERS: A Model for Watershed Planning, *Transactions of the*  
853 *ASAE*, 23, 938–944, <https://doi.org/10.13031/2013.34692>, 1980.

854 Bernhard, N., Moskwa, L.-M., Schmidt, K., Oeser, R. A., Aburto, F., Bader, M. Y., Baumann, K., Blanckenburg, F.  
855 von, Boy, J., van den Brink, L., Brucker, E., Büdel, B., Canessa, R., Dippold, M. A., Ehlers, T. A., Fuentes, J. P.,  
856 Godoy, R., Jung, P., Karsten, U., Köster, M., Kuzyakov, Y., Leinweber, P., Neidhardt, H., Matus, F., Mueller,  
857 C. W., Oelmann, Y., Osés, R., Osses, P., Paulino, L., Samolov, E., Schaller, M., Schmid, M., Spielvogel, S.,  
858 Spohn, M., Stock, S., Stroncik, N., Tielbörger, K., Übernickel, K., Scholten, T., Seguel, O., Wagner, D., and  
859 Kühn, P.: Pedogenic and microbial interrelations to regional climate and local topography: New insights from  
860 a climate gradient (arid to humid) along the Coastal Cordillera of Chile, *CATENA*, 170, 335–355,  
861 <https://doi.org/10.1016/j.catena.2018.06.018>, 2018.

862 Beven, K. J. and Kirkby, M. J.: A physically based, variable contributing area model of basin hydrology / Un  
863 modèle à base physique de zone d'appel variable de l'hydrologie du bassin versant, *Hydrological Sciences*  
864 *Bulletin*, 24, 43–69, <https://doi.org/10.1080/02626667909491834>, 1979.

865 Black, T. A. and Montgomery, D. R.: Sediment transport by burrowing mammals, Marin County, California, *Earth*  
866 *Surf. Process. Landforms*, 16, 163–172, <https://doi.org/10.1002/esp.3290160207>, 1991.

867 Boudreau, B. P.: Mathematics of tracer mixing in sediments; I, Spatially-dependent, diffusive mixing, *American*  
868 *Journal of Science*, 286, 161–198, <https://doi.org/10.2475/ajs.286.3.161>, 1986.

- 869 Boudreau, B. P.: The diffusion and telegraph equations in diagenetic modelling, *Geochimica et Cosmochimica*  
870 *Acta*, 53, 1857–1866, [https://doi.org/10.1016/0016-7037\(89\)90306-2](https://doi.org/10.1016/0016-7037(89)90306-2), 1989.
- 871 Braun, J., Mercier, J., Guillocheau, F., and Robin, C.: A simple model for regolith formation by chemical  
872 weathering, *J. Geophys. Res. Earth Surf.*, 121, 2140–2171, <https://doi.org/10.1002/2016JF003914>, 2016.
- 873 Brosens, L., Campforts, B., Robinet, J., Vanacker, V., Opfergelt, S., Ameijeiras-Mariño, Y., Minella, J. P. G., and  
874 Govers, G.: Slope Gradient Controls Soil Thickness and Chemical Weathering in Subtropical Brazil:  
875 Understanding Rates and Timescales of Regional Soilscape Evolution Through a Combination of Field Data  
876 and Modeling, *J. Geophys. Res. Earth Surf.*, 125, 1, <https://doi.org/10.1029/2019JF005321>, 2020.
- 877 Carretier, S., Godd eris, Y., Delannoy, T., and Rouby, D.: Mean bedrock-to-saprolite conversion and erosion rates  
878 during mountain growth and decline, *Geomorphology*, 209, 39–52,  
879 <https://doi.org/10.1016/j.geomorph.2013.11.025>, 2014.
- 880 Cerqueira, R.: The Distribution of Didelphis in South America (Polyprotodontia, Didelphidae), *Journal of*  
881 *Biogeography*, 12, 135, <https://doi.org/10.2307/2844837>, 1985.
- 882 Chen, M., Ma, L., Shao, M. a., Wei, X., Jia, Y., Sun, S., Zhang, Q., Li, T., Yang, X., and Gan, M.: Chinese zokor  
883 (*Myospalax fontanierii*) excavating activities lessen runoff but facilitate soil erosion – A simulation  
884 experiment, *CATENA*, 202, 105248, <https://doi.org/10.1016/j.catena.2021.105248>, 2021.
- 885 Choi, K., Arnhold, S., Huwe, B., and Reineking, B.: Daily Based Morgan–Morgan–Finney (DMMF) Model: A  
886 Spatially Distributed Conceptual Soil Erosion Model to Simulate Complex Soil Surface Configurations,  
887 *Water*, 9, 278, <https://doi.org/10.3390/w9040278>, 2017.
- 888 Cohen, S., Willgoose, G., Svoray, T., Hancock, G., and Sela, S.: The effects of sediment transport, weathering, and  
889 aeolian mechanisms on soil evolution, *J. Geophys. Res. Earth Surf.*, 120, 260–274,  
890 <https://doi.org/10.1002/2014JF003186>, 2015.
- 891 Cohen, S., Willgoose, G., and Hancock, G.: The mARM3D spatially distributed soil evolution model: Three-  
892 dimensional model framework and analysis of hillslope and landform responses, *J. Geophys. Res.*, 115, 191,  
893 <https://doi.org/10.1029/2009JF001536>, 2010.
- 894 Coombes, M. A.: Biogeomorphology: diverse, integrative and useful, *Earth Surf. Process. Landforms*, 41, 2296–  
895 2300, <https://doi.org/10.1002/esp.4055>, 2016.
- 896 Corenblit, D., Corbara, B., and Steiger, J.: Biogeomorphological eco-evolutionary feedback between life and  
897 geomorphology: a theoretical framework using fossorial mammals, *Die Naturwissenschaften*, 108, 55,  
898 <https://doi.org/10.1007/s00114-021-01760-y>, 2021.
- 899 Debruyne, L. A.L. and Conacher, A. J.: The bioturbation activity of ants in agricultural and naturally vegetated  
900 habitats in semiarid environments, *Soil Res.*, 32, 555, <https://doi.org/10.1071/SR9940555>, 1994.
- 901 Devia, G. K., Ganasri, B. P., and Dwarakish, G. S.: A Review on Hydrological Models, *Aquatic Procedia*, 4, 1001–  
902 1007, <https://doi.org/10.1016/j.aqpro.2015.02.126>, 2015.
- 903 Durner, W., Iden, S. C., and Unold, G. von: The integral suspension pressure method (ISP) for precise particle-size  
904 analysis by gravitational sedimentation, *Water Resour. Res.*, 53, 33–48, <https://doi.org/10.1002/2016WR019830>,  
905 2017.
- 906 Eccard, J. A. and Herde, A.: Seasonal variation in the behaviour of a short-lived rodent, *BMC ecology*, 13, 43,  
907 <https://doi.org/10.1186/1472-6785-13-43>, 2013.
- 908 Ferro, L. I. and Barquez, R. M.: Species Richness of Nonvolant Small Mammals Along Elevational Gradients in  
909 Northwestern Argentina, *Biotropica*, 41, 759–767, <https://doi.org/10.1111/j.1744-7429.2009.00522.x>, 2009.
- 910 Foster, D. W.: BIOTURB: A FORTRAN program to simulate the effects of bioturbation on the vertical distribution  
911 of sediment, *Computers & Geosciences*, 11, 39–54, [https://doi.org/10.1016/0098-3004\(85\)90037-8](https://doi.org/10.1016/0098-3004(85)90037-8), 1985.

- 912 François, F., Poggiale, J.-C., Durbec, J.-P., and Stora, G.: A New Approach for the Modelling of Sediment  
 913 Reworking Induced by a Macrobenthic Community, *Acta Biotheoretica*, 45, 295–319,  
 914 <https://doi.org/10.1023/A:1000636109604>, 1997.
- 915 Gabet, E. J.: Gopher bioturbation: field evidence for non-linear hillslope diffusion, *Earth Surf. Process. Landforms*,  
 916 25, 1419–1428, [https://doi.org/10.1002/1096-9837\(200012\)25:13<1419:AID-ESP148>3.0.CO;2-1](https://doi.org/10.1002/1096-9837(200012)25:13<1419:AID-ESP148>3.0.CO;2-1), 2000.
- 917 Gabet, E. J., Perron, J. T., and Johnson, D. L.: Biotic origin for Mima mounds supported by numerical modeling,  
 918 *Geomorphology*, 206, 58–66, <https://doi.org/10.1016/j.geomorph.2013.09.018>, 2014.
- 919 Gabet, E. J., Reichman, O. J., and Seabloom, E. W.: The Effects of Bioturbation on Soil Processes and Sediment  
 920 Transport, *Annu. Rev. Earth Planet. Sci.*, 31, 249–273, <https://doi.org/10.1146/annurev.earth.31.100901.141314>,  
 921 2003.
- 922 Gray, H. J., Keen-Zebert, A., Furbish, D. J., Tucker, G. E., and Mahan, S. A.: Depth-dependent soil mixing persists  
 923 across climate zones, *Proceedings of the National Academy of Sciences of the United States of America*, 117,  
 924 8750–8756, <https://doi.org/10.1073/pnas.1914140117>, 2020.
- 925 Grigusova, P., Larsen, A., Achilles, S., Brandl, R., del Río, C., Farwig, N., Kraus, D., Paulino, L., Plissock, P.,  
 926 Übernicker, K., and Bendix, J.: Higher sediment redistribution rates related to burrowing animals than  
 927 previously assumed as revealed by time-of-flight-based monitoring, *Earth Surf. Dynam.*, 10, 1273–1301,  
 928 <https://doi.org/10.5194/esurf-10-1273-2022>, 2022.
- 929 Grigusova, P., Larsen, A., Achilles, S., Klug, A., Fischer, R., Kraus, D., Übernicker, K., Paulino, L., Plissock, P.,  
 930 Brandl, R., Farwig, N., and Bendix, J.: Area-Wide Prediction of Vertebrate and Invertebrate Hole Density and  
 931 Depth across a Climate Gradient in Chile Based on UAV and Machine Learning, *Drones*, 5, 86,  
 932 <https://doi.org/10.3390/drones5030086>, 2021.
- 933 Hakonson, T. E.: The Effects of Pocket Gopher Burrowing on Water Balance and Erosion from Landfill Covers, *J.*  
 934 *environ. qual.*, 28, 659–665, <https://doi.org/10.2134/jeq1999.00472425002800020033x>, 1999.
- 935 Hall, K., Boelhouwers, J., and Driscoll, K.: Animals as Erosion Agents in the Alpine Zone: Some Data and  
 936 Observations from Canada, Lesotho, and Tibet, *Arctic, Antarctic, and Alpine Research*, 31, 436–446,  
 937 <https://doi.org/10.1080/15230430.1999.12003328>, 1999.
- 938 Hancock, G. and Lowry, J.: Quantifying the influence of rainfall, vegetation and animals on soil erosion and  
 939 hillslope connectivity in the monsoonal tropics of northern Australia, *Earth Surf. Process. Landforms*, 46,  
 940 2110–2123, <https://doi.org/10.1002/esp.5147>, 2021.
- 941 Hazelhoff, L., van Hoof, P., Imeson, A. C., and Kwaad, F. J. P. M.: The exposure of forest soil to erosion by  
 942 earthworms, *Earth Surf. Process. Landforms*, 6, 235–250, <https://doi.org/10.1002/esp.3290060305>, 1981.
- 943 Horn, B.K.P.: Hill shading and the reflectance map, *Proc. IEEE*, 69, 14–47,  
 944 <https://doi.org/10.1109/PROC.1981.11918>, 1981.
- 945 Imeson, A. C. and Kwaad, F. J. P. M.: Some Effects of Burrowing Animals on Slope Processes in the Luxembourg  
 946 Ardennes, *Geografiska Annaler: Series A, Physical Geography*, 58, 317–328,  
 947 <https://doi.org/10.1080/04353676.1976.11879941>, 1976.
- 948 Istanbuluoglu, E.: Vegetation-modulated landscape evolution: Effects of vegetation on landscape processes,  
 949 drainage density, and topography, *J. Geophys. Res.*, 110, 11, <https://doi.org/10.1029/2004JF000249>, 2005.
- 950 Jimenez, J. E., Feinsinger, P., and Jaksi, F. M.: Spatiotemporal Patterns of an Irruption and Decline of Small  
 951 Mammals in Northcentral Chile, *Journal of Mammalogy*, 73, 356–364, <https://doi.org/10.2307/1382070>, 1992.
- 952 Jong, S. M. de, Paracchini, M. L., Bertolo, F., Folving, S., Megier, J., and Roo, A.P.J. de: Regional assessment of soil  
 953 erosion using the distributed model SEMMED and remotely sensed data, *CATENA*, 37, 291–308,  
 954 [https://doi.org/10.1016/S0341-8162\(99\)00038-7](https://doi.org/10.1016/S0341-8162(99)00038-7), 1999.

- 955 Jumars, P. A., Nowell, A. R.M., and Self, R. F.L.: A simple model of flow —Sediment—Organism interaction,  
956 *Marine Geology*, 42, 155–172, [https://doi.org/10.1016/0025-3227\(81\)90162-6](https://doi.org/10.1016/0025-3227(81)90162-6), 1981.
- 957 Kadko, D. and Heath, G. R.: Models of depth-dependent bioturbation at MANOP Site H in the eastern equatorial  
958 Pacific, *J. Geophys. Res.*, 89, 6567, <https://doi.org/10.1029/JC089iC04p06567>, 1984.
- 959 Katzman, E. A., Zaytseva, E. A., Feoktistova, N. Y., Tovpinetz, N. N., Bogomolov, P. L., Potashnikova, E. V., and  
960 Surov, A. V.: Seasonal Changes in Burrowing of the Common Hamster (*Cricetus cricetus* L., 1758) (Rodentia:  
961 Cricetidae) in the City, *PJE*, 17, 251–258, <https://doi.org/10.18500/1684-7318-2018-3-251-258>, 2018.
- 962 Kinlaw, A. and Grasmueck, M.: Evidence for and geomorphologic consequences of a reptilian ecosystem  
963 engineer: The burrowing cascade initiated by the Gopher Tortoise, *Geomorphology*, 157–158, 108–121,  
964 <https://doi.org/10.1016/j.geomorph.2011.06.030>, 2012.
- 965 Kirols, H. S., Kevorkov, D., Uihlein, A., and Medraj, M.: The effect of initial surface roughness on water droplet  
966 erosion behaviour, *Wear*, 342–343, 198–209, <https://doi.org/10.1016/j.wear.2015.08.019>, 2015.
- 967 Kraus, D., Brandl, R., Achilles, S., Bendix, J., Grigusova, P., Larsen, A., Pliscoff, P., Übernickel, K., and Farwig, N.:  
968 Vegetation and vertebrate abundance as drivers of bioturbation patterns along a climate gradient, *PloS one*,  
969 17, e0264408, <https://doi.org/10.1371/journal.pone.0264408>, 2022.
- 970 Kügler, M., Hoffmann, T. O., Beer, A. R., Übernickel, K., Ehlers, T. A., Scherler, D., and Eichel, J.: (LiDAR) 3D  
971 Point Clouds and Topographic Data from the Chilean Coastal Cordillera, 2022.
- 972 La Croix, A. D., Gingras, M. K., Dashtgard, S. E., and Pemberton, S. G.: Computer modeling bioturbation: The  
973 creation of porous and permeable fluid-flow pathways, *Bulletin*, 96, 545–556,  
974 <https://doi.org/10.1306/07141111038>, 2012.
- 975 Larsen, A., Nardin, W., Lageweg, W. I., and Bätz, N.: Biogeomorphology, quo vadis? On processes, time, and  
976 space in biogeomorphology, *Earth Surf. Process. Landforms*, 46, 12–23, <https://doi.org/10.1002/esp.5016>, 2021.
- 977 Le Hir, P., Monbet, Y., and Orvain, F.: Sediment erodability in sediment transport modelling: Can we account for  
978 biota effects?, *Continental Shelf Research*, 27, 1116–1142, <https://doi.org/10.1016/j.csr.2005.11.016>, 2007.
- 979 Lehnert, L. W., Thies, B., Trachte, K., Achilles, S., Osses, P., Baumann, K., Schmidt, J., Samolov, E., Jung, P.,  
980 Leinweber, P., Karsten, U., Büdel, B., and Bendix, J.: A Case Study on Fog/Low Stratus Occurrence at Las  
981 Lomitas, Atacama Desert (Chile) as a Water Source for Biological Soil Crusts, *Aerosol Air Qual. Res.*, 18, 254–  
982 26, <https://doi.org/10.4209/aaqr.2017.01.0021>, 2018.
- 983 Li, G., Li, X., Li, J., Chen, W., Zhu, H., Zhao, J., and Hu, X.: Influences of Plateau Zokor Burrowing on Soil Erosion  
984 and Nutrient Loss in Alpine Meadows in the Yellow River Source Zone of West China, *Water*, 11, 2258,  
985 <https://doi.org/10.3390/w11112258>, 2019a.
- 986 Li, T. C., Shao, M. A., Jia, Y. H., Jia, X. X., Huang, L. M., and Gan, M.: Small-scale observation on the effects of  
987 burrowing activities of ants on soil hydraulic processes, *Eur J Soil Sci*, 70, 236–244,  
988 <https://doi.org/10.1111/ejss.12748>, 2019b.
- 989 Li, T., Shao, M. a., Jia, Y., Jia, X., and Huang, L.: Small-scale observation on the effects of the burrowing activities  
990 of mole crickets on soil erosion and hydrologic processes, *Agriculture, Ecosystems & Environment*, 261, 136–  
991 143, <https://doi.org/10.1016/j.agee.2018.04.010>, 2018.
- 992 Li, Z. and Zhang, J.: Calculation of Field Manning’s Roughness Coefficient, *Agricultural Water Management*, 49,  
993 153–161, [https://doi.org/10.1016/S0378-3774\(00\)00139-6](https://doi.org/10.1016/S0378-3774(00)00139-6), 2001.
- 994 Lilhare, R., Garg, V., and Nikam, B. R.: Application of GIS-Coupled Modified MMF Model to Estimate Sediment  
995 Yield on a Watershed Scale, *J. Hydrol. Eng.*, 20, 745, [https://doi.org/10.1061/\(ASCE\)HE.1943-5584.0001063](https://doi.org/10.1061/(ASCE)HE.1943-5584.0001063),  
996 2015.

- 997 López-Vicente, M., Navas, A., and Machín, J.: Modelling soil detachment rates in rainfed agrosystems in the  
998 south-central Pyrenees, *Agricultural Water Management*, 95, 1079–1089,  
999 <https://doi.org/10.1016/j.agwat.2008.04.004>, 2008.
- 1000 Malizia, A. I.: Population dynamics of the fossorial rodent *Ctenomys talarum* (Rodentia: Octodontidae), *Journal*  
1001 *of Zoology*, 244, 545–551, <https://doi.org/10.1111/j.1469-7998.1998.tb00059.x>, 1998.
- 1002 Meserve, P. L.: Trophic Relationships among Small Mammals in a Chilean Semiarid Thorn Scrub Community,  
1003 *Journal of Mammalogy*, 62, 304–314, <https://doi.org/10.2307/1380707>, 1981.
- 1004 Meyer, H., Reudenbach, C., Hengl, T., Katurji, M., and Nauss, T.: Improving performance of spatio-temporal  
1005 machine learning models using forward feature selection and target-oriented validation, *Environmental*  
1006 *Modelling & Software*, 101, 1–9, <https://doi.org/10.1016/j.envsoft.2017.12.001>, 2018.
- 1007 Meysman, F. J. R., Boudreau, B. P., and Middelburg, J. J.: Relations between local, nonlocal, discrete and  
1008 continuous models of bioturbation, *J Mar Res*, 61, 391–410, <https://doi.org/10.1357/002224003322201241>, 2003.
- 1009 Milstead, W. B., Meserve, P. L., Campanella, A., Previtali, M. A., Kelt, D. A., and Gutiérrez, J. R.: Spatial Ecology  
1010 of Small Mammals in North-central Chile: Role of Precipitation and Refuges, *Journal of Mammalogy*, 88,  
1011 1532–1538, <https://doi.org/10.1644/16-MAMM-A-407R.1>, 2007.
- 1012 Monteverde, M. J. and Piudo, L.: Activity Patterns of the Culpeo Fox (*Lycalopex Culpaeus Magellanica*) in a  
1013 Non-Hunting Area of Northwestern Patagonia, Argentina, *Mammal Study*, 36, 119–125,  
1014 <https://doi.org/10.3106/041.036.0301>, 2011.
- 1015 Morgan, R. P. C. and Duzant, J. H.: Modified MMF (Morgan–Morgan–Finney) model for evaluating effects of  
1016 crops and vegetation cover on soil erosion, *Earth Surf. Process. Landforms*, 33, 90–106,  
1017 <https://doi.org/10.1002/esp.1530>, 2008.
- 1018 Morgan, R. P. C., Quinton, J. N., Smith, R. E., Govers, G., Poesen, J. W. A., Auerswald, K., Chisci, G., Torri, D., and  
1019 Styczen, M. E.: The European Soil Erosion Model (EUROSEM): a dynamic approach for predicting sediment  
1020 transport from fields and small catchments, *Earth Surf. Process. Landforms*, 23, 527–544,  
1021 [https://doi.org/10.1002/\(SICI\)1096-9837\(199806\)23:6<527:AID-ESP868>3.0.CO;2-5](https://doi.org/10.1002/(SICI)1096-9837(199806)23:6<527:AID-ESP868>3.0.CO;2-5), 1998.
- 1022 Morgan, R.P.C.: A simple approach to soil loss prediction: a revised Morgan–Morgan–Finney model, *CATENA*,  
1023 44, 305–322, [https://doi.org/10.1016/S0341-8162\(00\)00171-5](https://doi.org/10.1016/S0341-8162(00)00171-5), 2001.
- 1024 Morgan, R.P.C., Morgan, D.D.V., and Finney, H. J.: A predictive model for the assessment of soil erosion risk,  
1025 *Journal of Agricultural Engineering Research*, 30, 245–253, [https://doi.org/10.1016/S0021-8634\(84\)80025-6](https://doi.org/10.1016/S0021-8634(84)80025-6),  
1026 1984.
- 1027 Nearing, M. A., Foster, G. R., Lane, L. J., and Finkner, S. C.: A Process-Based Soil Erosion Model for USDA-Water  
1028 Erosion Prediction Project Technology, *Transactions of the ASAE*, 32, 1587–1593,  
1029 <https://doi.org/10.13031/2013.31195>, 1989.
- 1030 Nkem, J. N., Lobry de Bruyn, L. A., Grant, C. D., and Hulugalle, N. R.: The impact of ant bioturbation and  
1031 foraging activities on adjacent soil properties, *Pedobiologia*, 44, 609–621, [https://doi.org/10.1078/S0031-4056\(04\)70075-X](https://doi.org/10.1078/S0031-4056(04)70075-X), 2000.
- 1033 Oeser, R. A., Stroncik, N., Moskwa, L.-M., Bernhard, N., Schaller, M., Canessa, R., van den Brink, L., Köster, M.,  
1034 Brucker, E., Stock, S., Fuentes, J. P., Godoy, R., Matus, F. J., Osés Pedraza, R., Osses McIntyre, P., Paulino, L.,  
1035 Seguel, O., Bader, M. Y., Boy, J., Dippold, M. A., Ehlers, T. A., Kühn, P., Kuzyakov, Y., Leinweber, P.,  
1036 Scholten, T., Spielvogel, S., Spohn, M., Übernickel, K., Tielbörger, K., Wagner, D., and Blanckenburg, F. von:  
1037 Chemistry and microbiology of the Critical Zone along a steep climate and vegetation gradient in the Chilean  
1038 Coastal Cordillera, *CATENA*, 170, 183–203, <https://doi.org/10.1016/j.catena.2018.06.002>, 2018.
- 1039 Orvain, F., Sauriau, P.-G., Bacher, C., and Prineau, M.: The influence of sediment cohesiveness on bioturbation  
1040 effects due to *Hydrobia ulvae* on the initial erosion of intertidal sediments: A study combining flume and  
1041 model approaches, *Journal of Sea Research*, 55, 54–73, <https://doi.org/10.1016/j.seares.2005.10.002>, 2006.



- 1042 Pelletier, J. D., Barron-Gafford, G. A., Breshears, D. D., Brooks, P. D., Chorover, J., Durcik, M., Harman, C. J.,  
 1043 Huxman, T. E., Lohse, K. A., Lybrand, R., Meixner, T., McIntosh, J. C., Papuga, S. A., Rasmussen, C., Schaap,  
 1044 M., Swetnam, T. L., and Troch, P. A.: Coevolution of nonlinear trends in vegetation, soils, and topography  
 1045 with elevation and slope aspect: A case study in the sky islands of southern Arizona, *J. Geophys. Res. Earth*  
 1046 *Surf.*, 118, 741–758, <https://doi.org/10.1002/jgrf.20046>, 2013.
- 1047 Penman, H.: Natural evaporation from open water, bare soil and grass, *Proceedings of the Royal Society of*  
 1048 *London. Series A, Mathematical and physical sciences*, 193, 120–145, <https://doi.org/10.1098/rspa.1948.0037>,  
 1049 1948.
- 1050 Pollacco, J. A. P.: A generally applicable pedotransfer function that estimates field capacity and permanent  
 1051 wilting point from soil texture and bulk density, *Can. J. Soil. Sci.*, 88, 761–774,  
 1052 <https://doi.org/10.4141/CJSS07120>, 2008.
- 1053 Qin, Y., Yi, S., Ding, Y., Qin, Y., Zhang, W., Sun, Y., Hou, X., Yu, H., Meng, B., Zhang, H., Chen, J., and Wang, Z.:  
 1054 Effects of plateau pikas' foraging and burrowing activities on vegetation biomass and soil organic carbon of  
 1055 alpine grasslands, *Plant Soil*, 458, 201–216, <https://doi.org/10.1007/s11104-020-04489-1>, 2021.
- 1056 Reichman, O. J. and Seabloom, E. W.: The role of pocket gophers as subterranean ecosystem engineers, *Trends in*  
 1057 *Ecology & Evolution*, 17, 44–49, [https://doi.org/10.1016/S0169-5347\(01\)02329-1](https://doi.org/10.1016/S0169-5347(01)02329-1), 2002.
- 1058 Renard, K., Foster, G., Weesies, G., and Porter, J.: RUSLE: The Revised Universal Soil Loss Equation, *Journal of*  
 1059 *Soil Water Conservation*, 30–33, 1991.
- 1060 Ridd, P. V.: Flow Through Animal Burrows in Mangrove Creeks, *Estuarine, Coastal and Shelf Science*, 43, 617–  
 1061 625, <https://doi.org/10.1006/ecss.1996.0091>, 1996.
- 1062 Rodríguez-Caballero, E., Cantón, Y., Chamizo, S., Afana, A., and Solé-Benet, A.: Effects of biological soil crusts on  
 1063 surface roughness and implications for runoff and erosion, *Geomorphology*, 145–146, 81–89,  
 1064 <https://doi.org/10.1016/j.geomorph.2011.12.042>, 2012.
- 1065 Román-Sánchez, A., Reimann, T., Wallinga, J., and Vanwalleghem, T.: Bioturbation and erosion rates along the  
 1066 soil-hillslope conveyor belt, part 1: Insights from single-grain feldspar luminescence, *Earth Surf. Process.*  
 1067 *Landforms*, 44, 2051–2065, <https://doi.org/10.1002/esp.4628>, 2019.
- 1068 ROO, A. P. J. de, WESSELING, C. G., and RITSEMA, C. J.: LISEM: A SINGLE-EVENT PHYSICALLY BASED  
 1069 HYDROLOGICAL AND SOIL EROSION MODEL FOR DRAINAGE BASINS. I: THEORY, INPUT AND  
 1070 OUTPUT, *Hydrol. Process.*, 10, 1107–1117, [https://doi.org/10.1002/\(SICI\)1099-1085\(199608\)10:8<1107:AID-  
 1071 HYP415>3.0.CO;2-4](https://doi.org/10.1002/(SICI)1099-1085(199608)10:8<1107:AID-HYP415>3.0.CO;2-4), 1996.
- 1072 Rutin, J.: The burrowing activity of scorpions (*Scorpio maurus palmatus*) and their potential contribution to the  
 1073 erosion of Hamra soils in Karkur, central Israel, *Geomorphology*, 15, 159–168, [https://doi.org/10.1016/0169-  
 1074 555X\(95\)00120-T](https://doi.org/10.1016/0169-555X(95)00120-T), 1996.
- 1075 Sanford, L. P.: Modeling a dynamically varying mixed sediment bed with erosion, deposition, bioturbation,  
 1076 consolidation, and armoring, *Computers & Geosciences*, 34, 1263–1283,  
 1077 <https://doi.org/10.1016/j.cageo.2008.02.011>, 2008.
- 1078 Schiffers, K., Teal, L. R., Travis, J. M. J., and Solan, M.: An open source simulation model for soil and sediment  
 1079 bioturbation, *PloS one*, 6, e28028, <https://doi.org/10.1371/journal.pone.0028028>, 2011.
- 1080 Shannon, C. E.: A Mathematical Theory of Communication, *Bell System Technical Journal*, 27, 379–423,  
 1081 <https://doi.org/10.1002/j.1538-7305.1948.tb01338.x>, 1948.
- 1082 Shull, D. H.: Transition-matrix model of bioturbation and radionuclide diagenesis, *Limnol. Oceanogr.*, 46, 905–  
 1083 916, <https://doi.org/10.4319/lo.2001.46.4.0905>, 2001.
- 1084 Simonetti, J. A.: Microhabitat Use by Small Mammals in Central Chile, *Oikos*, 56, 309,  
 1085 <https://doi.org/10.2307/3565615>, 1989.

- 1086 Soetaert, K., Herman, P. M. J., Middelburg, J. J., Heip, C., deStigter, H. S., van Weering, T. C. E., Epping, E., and  
 1087 Helder, W.: Modeling  $^{210}\text{Pb}$ -derived mixing activity in ocean margin sediments: Diffusive versus nonlocal  
 1088 mixing, *J Mar Res*, 54, 1207–1227, <https://doi.org/10.1357/0022240963213808>, 1996.
- 1089 Taylor, A. R., Lenoir, L., Vegerfors, B., and Persson, T.: Ant and Earthworm Bioturbation in Cold-Temperate  
 1090 Ecosystems, *Ecosystems*, 22, 981–994, <https://doi.org/10.1007/s10021-018-0317-2>, 2019.
- 1091 Temme, A. J.A.M. and Vanwallegem, T.: LORICA – A new model for linking landscape and soil profile  
 1092 evolution: Development and sensitivity analysis, *Computers & Geosciences*, 90, 131–143,  
 1093 <https://doi.org/10.1016/j.cageo.2015.08.004>, 2016.
- 1094 Tews, J., Brose, U., Grimm, V., Tielbörger, K., Wichmann, M. C., Schwager, M., and Jeltsch, F.: Animal species  
 1095 diversity driven by habitat heterogeneity/diversity: the importance of keystone structures, *Journal of*  
 1096 *Biogeography*, 31, 79–92, <https://doi.org/10.1046/j.0305-0270.2003.00994.x>, 2004.
- 1097 Tomasella, J., Hodnett, M. G., and Rossato, L.: Pedotransfer Functions for the Estimation of Soil Water Retention  
 1098 in Brazilian Soils, *Soil Sci. Soc. Am. J.*, 64, 327–338, <https://doi.org/10.2136/sssaj2000.641327x>, 2000.
- 1099 Trauth, M. H.: TURBO: a dynamic-probabilistic simulation to study the effects of bioturbation on  
 1100 paleoceanographic time series, *Computers & Geosciences*, 24, 433–441, [https://doi.org/10.1016/S0098-3004\(98\)00019-3](https://doi.org/10.1016/S0098-3004(98)00019-3), 1998.
- 1102 Tucker, G. E. and Hancock, G. R.: Modelling landscape evolution, *Earth Surf. Process. Landforms*, 35, 28–50,  
 1103 <https://doi.org/10.1002/esp.1952>, 2010.
- 1104 Übernichel, K., Pizarro-Araya, J., Bhagavathula, S., Paulino, L., and Ehlers, T. A.: Reviews and syntheses:  
 1105 Composition and characteristics of burrowing animals along a climate and ecological gradient, Chile,  
 1106 *Biogeosciences*, 18, 5573–5594, <https://doi.org/10.5194/bg-18-5573-2021>, 2021a.
- 1107 Übernichel, K., Ehlers, T. A., Paulino, L., and Fuentes Espoz, J.-P.: Time series of meteorological stations on an  
 1108 elevational gradient in National Park La Campana, Chile, 2021b.
- 1109 Vanwallegem, T., Stockmann, U., Minasny, B., and McBratney, A. B.: A quantitative model for integrating  
 1110 landscape evolution and soil formation, *J. Geophys. Res. Earth Surf.*, 118, 331–347,  
 1111 <https://doi.org/10.1029/2011JF002296>, 2013.
- 1112 Vieira, D.C.S., Prats, S. A., Nunes, J. P., Shakesby, R. A., Coelho, C.O.A., and Keizer, J. J.: Modelling runoff and  
 1113 erosion, and their mitigation, in burned Portuguese forest using the revised Morgan–Morgan–Finney model,  
 1114 *Forest Ecology and Management*, 314, 150–165, <https://doi.org/10.1016/j.foreco.2013.12.006>, 2014.
- 1115 Vigiak, O., Okoba, B. O., Sterk, G., and Groenenberg, S.: Modelling catchment-scale erosion patterns in the East  
 1116 African Highlands, *Earth Surf. Process. Landforms*, 30, 183–196, <https://doi.org/10.1002/esp.1174>, 2005.
- 1117 Voiculescu, M., Ianăș, A.-N., and Germain, D.: Exploring the impact of snow vole (*Chionomys nivalis*) burrowing  
 1118 activity in the Făgăraș Mountains, Southern Carpathians (Romania): Geomorphic characteristics and  
 1119 sediment budget, *CATENA*, 181, 104070, <https://doi.org/10.1016/j.catena.2019.05.016>, 2019.
- 1120 Wang, B., Zheng, F., Römkens, M. J.M., and Darboux, F.: Soil erodibility for water erosion: A perspective and  
 1121 Chinese experiences, *Geomorphology*, 187, 1–10, <https://doi.org/10.1016/j.geomorph.2013.01.018>, 2013.
- 1122 Wei, X., Li, S., Yang, P., and Cheng, H.: Soil erosion and vegetation succession in alpine Kobresia steppe meadow  
 1123 caused by plateau pika—A case study of Nagqu County, Tibet, *Chin. Geograph.Sc.*, 17, 75–81,  
 1124 <https://doi.org/10.1007/s11769-007-0075-0>, 2007.
- 1125 Welivitiya, W. D. D. P., Willgoose, G. R., and Hancock, G. R.: A coupled soilscape–landform evolution model:  
 1126 model formulation and initial results, *Earth Surf. Dynam.*, 7, 591–607, <https://doi.org/10.5194/esurf-7-591-2019>, 2019.

- 1128 Wheatcroft, R. A., Jumars, P. A., Smith, C. R., and Nowell, A. R. M.: A mechanistic view of the particulate  
1129 biodiffusion coefficient: Step lengths, rest periods and transport directions, *J Mar Res*, 48, 177–207,  
1130 <https://doi.org/10.1357/002224090784984560>, 1990.
- 1131 Whitesides, C. J. and Butler, D. R.: Bioturbation by gophers and marmots and its effects on conifer germination,  
1132 *Earth Surf. Process. Landforms*, 41, 2269–2281, <https://doi.org/10.1002/esp.4046>, 2016.
- 1133 Wilkinson, M. T., Richards, P. J., and Humphreys, G. S.: Breaking ground: Pedological, geological, and ecological  
1134 implications of soil bioturbation, *Earth-Science Reviews*, 97, 257–272,  
1135 <https://doi.org/10.1016/j.earscirev.2009.09.005>, 2009.
- 1136 Williams, J. R. (Ed.): Sediment-yield prediction with Universal Equation using runoff energy factor. In Present  
1137 and prospective technology for predicting sediment yield and sources: Proceedings of the Sediment-Yield  
1138 Workshop, ARS-S-40, United States Department of Agriculture (USDA), New Orleans, USA, 1975.
- 1139 Wilson, M. F. J., O'Connell, B., Brown, C., Guinan, J. C., and Grehan, A. J.: Multiscale Terrain Analysis of  
1140 Multibeam Bathymetry Data for Habitat Mapping on the Continental Slope, *Marine Geodesy*, 30, 3–35,  
1141 <https://doi.org/10.1080/01490410701295962>, 2007.
- 1142 Wischmeier, W. and Smith, D. D.: Predicting rainfall erosion losses - A guide to conservation planning,  
1143 *Agriculture Handbook*, 1–58, 1978.
- 1144 Wood, S. N.: Generalized Additive Models, Chapman and Hall/CRC, 2006.
- 1145 Wösten, J.H.M. (Ed.): Soil Quality for Crop Production and Ecosystem Health, *Developments in Soil Science*,  
1146 Elsevier, 1997.
- 1147 Wu, C., Wu, H., Liu, D., Han, G., Zhao, P., and Kang, Y.: Crab bioturbation significantly alters sediment microbial  
1148 composition and function in an intertidal marsh, *Estuarine, Coastal and Shelf Science*, 249, 107116,  
1149 <https://doi.org/10.1016/j.ecss.2020.107116>, 2021.
- 1150 Yair, A.: Short and long term effects of bioturbation on soil erosion, water resources and soil development in an  
1151 arid environment, *Geomorphology*, 13, 87–99, [https://doi.org/10.1016/0169-555X\(95\)00025-Z](https://doi.org/10.1016/0169-555X(95)00025-Z), 1995.
- 1152 Yoo, K. and Mudd, S. M.: Toward process-based modeling of geochemical soil formation across diverse  
1153 landforms: A new mathematical framework, *Geoderma*, 146, 248–260,  
1154 <https://doi.org/10.1016/j.geoderma.2008.05.029>, 2008.
- 1155 Yoo, K., Amundson, R., Heimsath, A. M., and Dietrich, W. E.: Process-based model linking pocket gopher  
1156 (*Thomomys bottae*) activity to sediment transport and soil thickness, *J. Geophys. Res.*, 33, 917,  
1157 <https://doi.org/10.1130/G21831.1>, 2005.
- 1158 Yu, C., Zhang, J., Pang, X. P., Wang, Q., Zhou, Y. P., and Guo, Z. G.: Soil disturbance and disturbance intensity:  
1159 Response of soil nutrient concentrations of alpine meadow to plateau pika bioturbation in the Qinghai-  
1160 Tibetan Plateau, China, *Geoderma*, 307, 98–106, <https://doi.org/10.1016/j.geoderma.2017.07.041>, 2017.
- 1161 Zevenbergen, L. W. and Thorne, C. R.: Quantitative analysis of land surface topography, *Earth Surf. Process.*  
1162 *Landforms*, 12, 47–56, <https://doi.org/10.1002/esp.3290120107>, 1987.
- 1163 Zhang, Q., Li, J., Hu, G., and Zhang, Z.: Bioturbation potential of a macrofaunal community in Bohai Bay,  
1164 northern China, *Marine pollution bulletin*, 140, 281–286, <https://doi.org/10.1016/j.marpolbul.2019.01.063>, 2019.
- 1165 Zhang, S., Fang, X., Zhang, J., Yin, F., Zhang, H., Wu, L., and Kitazawa, D.: The Effect of Bioturbation Activity of  
1166 the Ark Clam *Scapharca subcrenata* on the Fluxes of Nutrient Exchange at the Sediment-Water Interface, *J.*  
1167 *Ocean Univ. China*, 19, 232–240, <https://doi.org/10.1007/s11802-020-4112-2>, 2020.
- 1168
- 1169